Cell Reports

Hypoxic preconditioning protects against ischemic kidney injury through the IDO1/kynurenine pathway

Graphical abstract

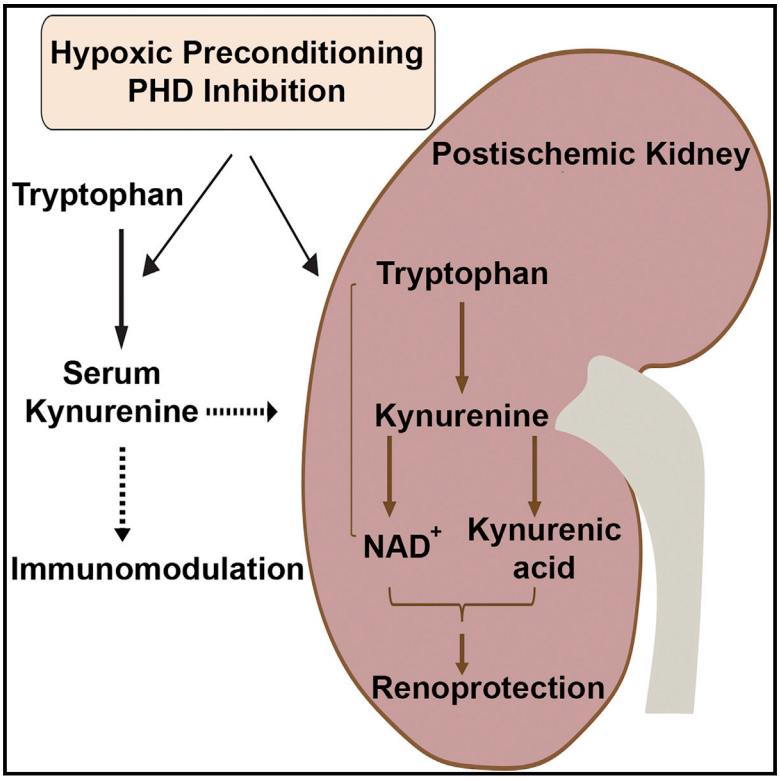

Authors

Rafael Torosyan, Shengping Huang, Prashant V. Bommi, ..., Peng Gao, Navdeep S. Chandel, Pinelopi P. Kapitsinou

Correspondence

pinelopi.kapitsinou@northwestern.edu

In brief

Torosyan et al. show that two potent cytoprotective strategies, hypoxic preconditioning and PHD inhibition, enhance kidney tissue resilience against ischemic injury by activating the kynurenine metabolic pathway. Specifically, they promote systemic kynurenine increase and enhance kynurenine metabolism, leading to preservation of NAD^+ and generation of kynurenic acid in the post-ischemic kidney.

Highlights

- Hypoxia and PHD inhibition increase serum kynurenine
- *Ido1* deficiency blunts the increase in serum kynurenine by hypoxia and PHD inhibition
- The IDO1-kynurenine axis is required in renoprotection by hypoxic preconditioning
- Hypoxia and PHD inhibition activate the kynurenine pathway in the post-ischemic kidney

Torosyan et al., 2021, Cell Reports *36*, 109547
August 17, 2021
https://doi.org/10.1016/j.celrep.2021.109547

CellPress

Cell Reports

CellPress
OPEN ACCESS

Report

Hypoxic preconditioning protects against ischemic kidney injury through the IDO1/kynurenine pathway

Rafael Torosyan,[1,9,10] Shengping Huang,[1,9,11] Prashant V. Bommi,[2,8] Ratnakar Tiwari,[2,8] Si Young An,[2,8] Michael Schonfeld,[1] Ganeshkumar Rajendran,[1] Matthew A. Kavanaugh,[1] Benjamin Gibbs,[1] Agnieszka D. Truax,[3] Samuel Bohney,[3] M. Wade Calcutt,[4] Evan W. Kerr,[5] Roberta Leonardi,[5] Peng Gao,[6] Navdeep S. Chandel,[6,7] and Pinelopi P. Kapitsinou[2,7,8,12,*]

[1]The Jared Grantham Kidney Institute, University of Kansas Medical Center, Kansas City, KS, USA
[2]Feinberg Cardiovascular and Renal Research Institute, Northwestern University Feinberg School of Medicine, Chicago, IL, USA
[3]Metabolon, Inc., Durham, NC, USA
[4]Vanderbilt Institute of Chemical Biology, Vanderbilt University, Nashville, TN, USA
[5]Department of Biochemistry, West Virginia University, Morgantown, WV, USA
[6]Robert H. Lurie Cancer Center Metabolomics Core, Northwestern University Feinberg School of Medicine, Chicago, IL, USA
[7]Department of Medicine and Robert H. Lurie Cancer Center, Northwestern University Feinberg School of Medicine, Chicago, IL, USA
[8]Division of Nephrology & Hypertension, Northwestern University Feinberg School of Medicine, Chicago, IL, USA
[9]These authors contributed equally
[10]Present address: Kansas City Kidney Consultants, Kansas City, MO, USA
[11]Present address: Department of Oral and Craniofacial Sciences, School of Dentistry, University of Missouri-Kansas City, MO, USA
[12]Lead contact
*Correspondence: pinelopi.kapitsinou@northwestern.edu
https://doi.org/10.1016/j.celrep.2021.109547

SUMMARY

Prolonged cellular hypoxia leads to energetic failure and death. However, sublethal hypoxia can trigger an adaptive response called hypoxic preconditioning. While prolyl-hydroxylase (PHD) enzymes and hypoxia-inducible factors (HIFs) have been identified as key elements of oxygen-sensing machinery, the mechanisms by which hypoxic preconditioning protects against insults remain unclear. Here, we perform serum metabolomic profiling to assess alterations induced by two potent cytoprotective approaches, hypoxic preconditioning and pharmacologic PHD inhibition. We discover that both approaches increase serum kynurenine levels and enhance kynurenine biotransformation, leading to preservation of NAD^+ in the post-ischemic kidney. Furthermore, we show that indoleamine 2,3-dioxygenase 1 (*Ido1*) deficiency abolishes the systemic increase of kynurenine and the subsequent renoprotection generated by hypoxic preconditioning and PHD inhibition. Importantly, exogenous administration of kynurenine restores the hypoxic preconditioning in the context of *Ido1* deficiency. Collectively, our findings demonstrate a critical role of the IDO1-kynurenine axis in mediating hypoxic preconditioning.

INTRODUCTION

Oxygen deprivation results in energy failure in cells and is associated with significant mortality in the context of ischemic disorders. Sublethal hypoxia can induce hypoxic preconditioning (HP), an evolutionarily conserved adaptive response that confers resistance to diverse cellular insults (Kapitsinou and Haase, 2015; Murry et al., 1986).

The cellular response to hypoxia is predominantly controlled by hypoxia-inducible factors (HIFs), transcription factors consisting of an oxygen-labile alpha subunit (HIF-α) and a stable beta subunit (HIF-β). Under normoxia, HIF-α is hydroxylated at specific proline residues by prolyl-4-hydroxylase domain (PHD) proteins 1–3 (Epstein et al., 2001; Schofield and Ratcliffe, 2004) and targeted for rapid proteasomal degradation. Under hypoxia, HIF-α subunits translocate to the nucleus, dimerize with HIF-β, and induce the expression of genes regulating cellular metabolism, angiogenesis, erythropoiesis, apoptosis, and proliferation (Majmundar et al., 2010; Semenza, 2012). Remarkably, HIF activation by pharmacologic PHD inhibition maintains tissue homeostasis in different models of organ injury, including acute kidney injury (AKI) (Bernhardt et al., 2006; Eltzschig et al., 2014; Hill et al., 2008; Kapitsinou et al., 2012; Olenchock et al., 2016).

Despite the organ-wide protection generated by activation of hypoxic signaling, gaps in understanding the underlying cellular and systemic mechanisms have hindered clinical translation. In the present study, we hypothesized that activation of hypoxia response leads to systemic metabolic alterations, which play a crucial role in mediating protection against ischemic kidney injury and inflammation. To test this hypothesis, we used metabolomic profiling to identify common alterations in serum metabolome induced by two cytoprotective approaches, HP and pharmacologic PHD inhibition. By integrating functional genomics

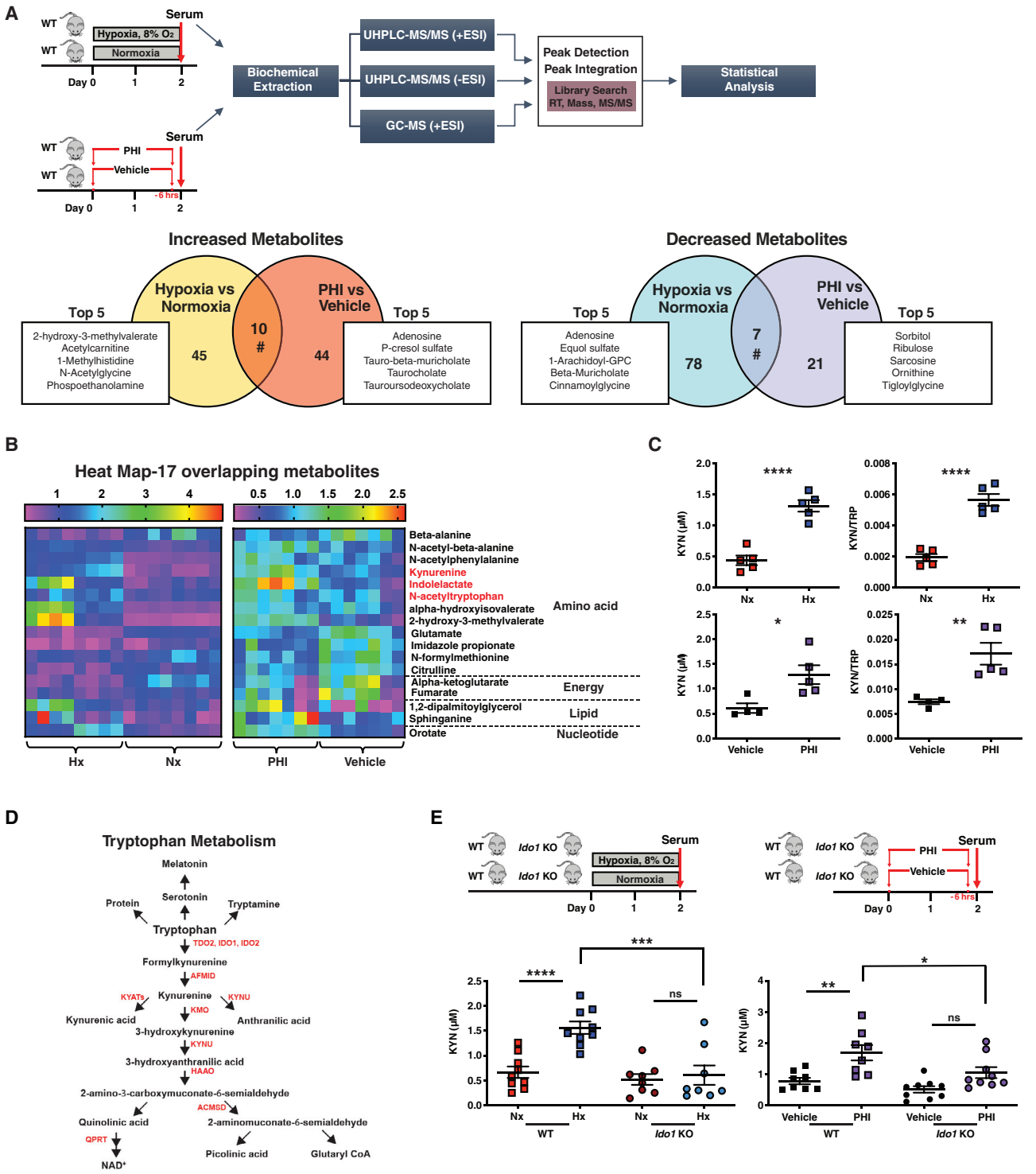

Figure 1. Hypoxia and pharmacologic PHD inhibition promote tryptophan metabolism to kynurenine in an IDO1-dependent manner

(A) Top graph summarizes the experimental workflow for the comparative metabolomic analysis of HP and pharmacologic PHD inhibition. Sera from mice exposed to 2 days of hypoxia 8% or two doses of PHI were analyzed using liquid chromatography-mass spectrometry (LC/MS) and gas chromatography-mass spectrometry (GC/MS) platforms. On the bottom, Venn diagrams show the differentially accumulated metabolite features, revealing uniquely or commonly increased (left graph) or decreased (right graph) metabolites under exposure to hypoxia versus normoxia and PHI versus vehicle. The top five uniquely regulated metabolites are listed for each condition in the attached boxes. n = 8 for HP and n = 7 for PHI.

(B) Heatmap visualization of the 17 overlapping metabolites between the two experimental sets (hypoxia versus normoxia and PHI versus vehicle).

(legend continued on next page)

studies, we identified a critical role for tryptophan metabolism in promoting resistance against post-ischemic kidney injury.

RESULTS

HP attenuates post-ischemic kidney injury and inflammation

While hypoxia is the major inhibitory stimulus of the PHD catalytic activity, the effect of hypoxia exposure as preconditioning against renal ischemia-reperfusion injury (IRI) has only recently been explored (Johnsen et al., 2020). To investigate the impact of HP on renal IRI outcomes, we used a model of normobaric hypoxia in which mice were subjected to 8% O_2 for 2 days. We have previously reported that this model activates HIF-signaling in the lungs (Kapitsinou et al., 2016). Furthermore, consistent with the activation of hypoxic response, renal erythropoietin (*Epo*) mRNA and serum Epo protein levels were increased 22- and 25-fold, respectively (Figure S1A). Following hypoxia exposure, mice were subjected to unilateral renal IRI and sacrificed on day 3 after IRI (Figure S1B). Remarkably, post-ischemic kidneys from HP mice showed attenuated kidney injury as indicated by significantly reduced injury scores and 2.3-fold suppression in kidney injury molecule 1 (*Kim1*) mRNA compared to normoxic controls. Furthermore, HP significantly reduced the infiltration of myeloid cells in post-ischemic kidneys by 85% and suppressed the expression of the proinflammatory genes vascular cell adhesion molecule 1 (*Vcam1*) and *Tnfa.* Taken together, these results suggest that HP protects against IRI-induced kidney injury and inflammation.

Hypoxia and pharmacologic inhibition of PHDs increase circulating levels of the tryptophan metabolite kynurenine

We have previously reported that pre-ischemic administration of PHD inhibitor (PHI) activates HIFs and attenuates post-ischemic renal injury and inflammation (Kapitsinou et al., 2012, 2014). To identify candidate metabolites involved in cytoprotection provided by HP and PHI, we compared alterations in serum metabolome induced by these approaches. Unbiased metabolomic profiling was performed by liquid chromatography-mass spectrometry (LC/MS) and gas chromatography-mass spectrometry (GC/MS) platforms (Figure 1A). Among 369 named biochemicals detected, 82 metabolites (54 upregulated and 28 downregulated) were determined to be significantly altered in the serum of PHI-treated mice compared to controls (Table S1). For the HP, we detected 362 named biochemicals, of which 140 (55 upregulated and 85 downregulated) were found to be significantly dysregulated in the serum of hypoxia exposed mice compared to controls (Figure 1A; Table S1). Notably, when we compared the significantly changed metabolites between the two datasets, we identified a high number of unique metabolomic alterations (118/135), of which 15 metabolites showed discordant changes (Figure 1A; data not shown). For instance, while PHI increased serum levels of pyruvate and ribose and reduced levels of ribulose, the opposite was the case in HP. These findings suggest that HP and PHI induced distinct metabolic changes in glucose metabolism. On the other hand, the presence of 17 overlapping metabolites revealed a shared metabolomic response between the two approaches, which mainly involved alterations in amino acid metabolism (Figure 1B). Among the overlapping metabolites, kynurenine, a breakdown product of tryptophan, showed a 2.7-fold and 1.8-fold increase, respectively, in HP and PHI compared to corresponding controls (Figure 1B). These results were validated by a targeted LC-MS/MS assay, which quantified serum kynurenine concentrations on independent experiments using a calibration curve made with known concentrations of kynurenine (Figure 1C). Consistently, the serum kynurenine to tryptophan ratio was significantly increased by both HP and PHD inhibition (Figure 1C), whereas no significant change in serum tryptophan levels was noted for both conditions (data not shown).

Ido1 deficiency abolishes the systemic accumulation of kynurenine and the subsequent renoprotection provided by HP and PHD inhibition

Most of the cellular free tryptophan (>95%) is degraded through the kynurenine pathway (KP) in which the rate-limiting step is the conversion of tryptophan to N-formylkynurenine. This reaction is catalyzed by either tryptophan-2,3-dioxygenase (TDO2) mainly in liver or indoleamine-2,3-dioxygenase (IDO1 and the more recently discovered IDO2) extrahepatically (Cervenka et al., 2017) (Figure 1D). To assess how HP and PHI increased serum kynurenine levels, we quantified the transcripts of several genes encoding KP enzymes in liver, kidney, and lung, tissues with robust transcriptional responses to activation of hypoxia signaling. In the liver, where most of the tryptophan degradation occurs through Tdo2 under normal conditions, neither HP nor PHI induced *Tdo2* mRNA (Figure S2A). In fact, we detected a minor suppression in *Tdo2* by PHI and a 1.8-fold reduction in *Ido2* transcript by HP, whereas hepatic expression levels for *Ido1* were too low to analyze. Notably, an upward trend was detected for renal *Ido1* by both HP and PHI but did not reach statistical significance. Among the differentially expressed KP genes in the lung, *Ido1* mRNA was significantly upregulated by PHI (Figure S2A). Overall, while there was not a uniform pattern of transcriptional responses in KP genes, the lack of induction in hepatic *Tdo2* suggested an extrahepatic mechanism for the serum kynurenine increase by HP and PHI.

To examine whether reduced degradation drives the increase in serum kynurenine by HP and PHI, we used a semiquantitative high-performance liquid chromatography (HPLC) tandem mass

(C) Serum kynurenine (KYN) concentration and kynurenine/tryptophan (KYN/TRP) ratio in the indicated conditions. n = 5 for HP and n = 4 (vehicle) and 5 (PHI).
(D) Diagram of the tryptophan metabolic pathway.
(E) Upper schemes illustrate the experimental protocols employed. Lower graphs show the serum kynurenine concentrations in wild-type (WT) and *Ido1* KO mice exposed to hypoxia (left) or PHI (right) compared to corresponding controls. n = 9 (WT, Nx and WT, Hx) and n= 8 (*Ido1* KO, Hx and *Ido1* KO, Nx).
Error bars represent SEM. For (A) and (B), statistics were determined using Welch's two-sample t tests and random effects ANOVA. For (C), two-tailed t test was used. For (E), statistics were determined using one-way ANOVA with Sidak correction. *p < 0.05; **p < 0.01; ***p < 0.001; ****p < 0.0001; ns, not statistically significant. Nx, normoxia; Hx, hypoxia; PHI, prolyl-hydroxylase inhibitor; WT, wild-type; KYN, kynurenine; KYN/TRP: kynurenine/tryptophan.

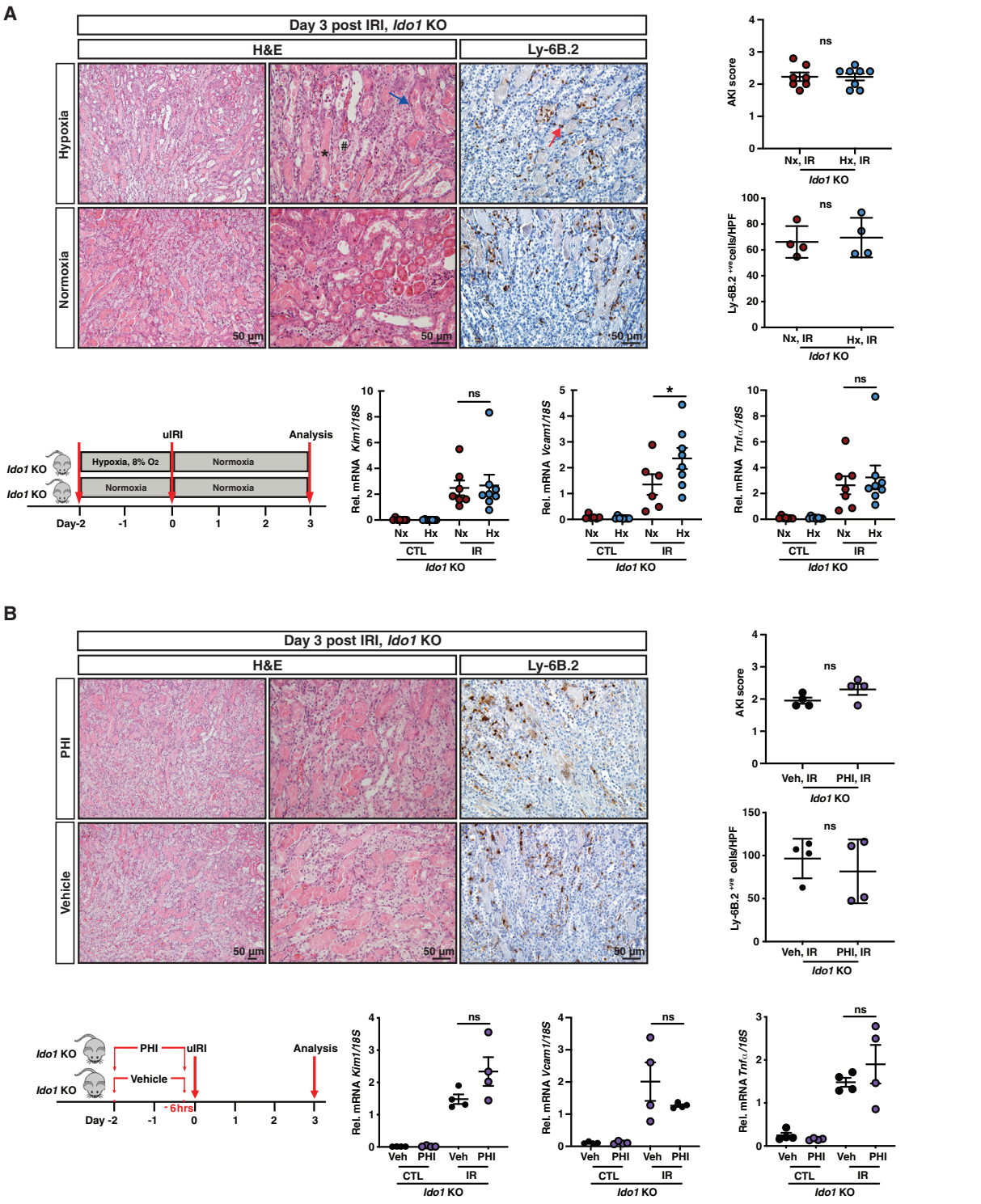

Figure 2. IDO1 deficiency abolishes the renoprotective and anti-inflammatory effects mediated by HP and pharmacologic PHD inhibition against renal IRI

(A and B) Overview of the experimental protocol and representative images of H&E- and Ly-6B.2-stained sections of day 3 post-IRI kidneys from *Ido1* KO mice subjected to HP compared to normoxia (A) or PHD inhibition compared to vehicle (B). Asterisk points to a tubule with cast formation, # indicates a dilated tubule, the blue arrow points to necrosis, and the red arrow points to a Ly-6B.2^{+ve} cell. Right panels demonstrate scoring of tubular injury and quantification of Ly-6B.2^{+ve}

(legend continued on next page)

spectrometry (MS/MS)-based assay to measure the levels of downstream KP metabolites. Compared to normoxia, the serum increase in kynurenine by hypoxia was associated with 34% increase in the serum levels of xanthurenic acid (XA), a metabolite formed by transamination of 3-hydroxykynurenine (3-HK) (Figure S2B). Furthermore, modest reductions were noted for the metabolites downstream of 3-HK, 3-hydroxyanthranilic acid (3-HAA), quinolinic acid (QUIN), and picolinic acid (PIC). In the setting of PHI, besides the expected increase in serum kynurenine, the other metabolites showed no significant changes (Figure S2B). For the kidney, hypoxia led to 54% reduction in 3-HAA, while QUIN and PIC showed significant increases (by 22% and 61%, respectively) compared to normoxia. Treatment with PHI led to significant increases of kynurenine (by 119%) and QUIN (by 14%) in kidney tissue compared to vehicle. Neither hypoxia nor PHI changed significantly the kidney NAD^+, which was validated by an independent biochemical assay (Figure S2C). Overall, these results rule out significant inhibition of kynurenine degradation by HP and PHI. Finally, serum blood urea nitrogen (BUN) levels remained normal following HP and PHI (Figure S2D), excluding reduced kidney function leading to kynurenine accumulation.

Because IDO1 is a rate-limiting enzyme in the conversion of tryptophan to kynurenine in extrahepatic tissues, we next examined the role of IDO1 in regulating serum kynurenine levels in the setting of hypoxic and pharmacologic PHD inhibition (Figure 1E). To this end, we used mice with germline inactivation of *Ido1* (Baban et al., 2004). Under normoxia, *Ido1* knockout (KO) mice had serum kynurenine levels comparable to wild-type mice, but upon exposure to hypoxia, they did not show a significant increase in serum kynurenine levels compared to normoxic littermates (Figure 1E). Likewise, *Ido1* KO mice treated with PHI failed to reach serum kynurenine levels observed in PHI-treated wild-type mice (Figure 1E). Therefore, these data indicate that *Ido1* drives the increase in serum kynurenine induced by both HP and PHI. Nevertheless, we cannot exclude that additional enzymatic activities in tryptophan metabolism may contribute to serum kynurenine levels following HP and PHD inhibition.

We next investigated whether the IDO1-dependent increase in serum kynurenine following HP or PHI was critical for the renoprotection generated by these approaches. Remarkably, post-IRI kidneys from *Ido1* KO mice subjected to HP showed comparable injury with non-preconditioned controls as indicated by *Kim1* mRNA and tubular injury scores (Figure 2A). Furthermore, infiltration by Ly6-B.2^{+ve} cells and *Tnfa* mRNA were not reduced by HP in *Ido1* KO mice, whereas *Vcam1* transcript was upregulated by 1.8-fold. Accordingly, PHI failed to attenuate post-ischemic kidney injury and inflammation in *Ido1* KO mice based on *Kim-1*, *Vcam1*, and *Tnfa* transcripts; tubular injury scores; and quantitative analysis of Ly6.$B2^{+ve}$ cells in post-ischemic kidneys compared to corresponding controls (Figure 2B). The lack of renoprotection in *Ido1* KO mice was in sharp contrast to our prior studies on wild-type mice. In summary, the IDO1-kynurenine axis is essential in renoprotection provided by HP and pharmacologic PHD inhibition.

Administration of kynurenine restores the HP in the context of Ido1 deficiency

We next wished to determine whether exogenous administration of kynurenine in hypoxia exposed *Ido1* KO mice restores the HP-induced renoprotection. Therefore, we injected *Ido1* KO mice subjected to HP with intraperitoneal (i.p.) kynurenine (50 mg/kg) 2 h prior to renal IRI, which led to serum kynurenine levels comparable to hypoxia and PHI (Figure S3A). Remarkably, administration of kynurenine ameliorated tissue injury in *Ido1* KO mice subjected to HP resulting in significantly reduced tubular injury scores and *Kim1* transcript levels compared to vehicle/HP-treated *Ido1* KO mice (Figure 3A). Furthermore, in addition to an 87% reduction in infiltration by Ly6.$B2^{+ve}$ cells, *Ido1* KO mice subjected to HP and kynurenine administration had 3.8-fold and 3.0-fold suppression in *Vcam1* and *Tnfa* mRNA, respectively, compared to post-IRI kidneys of vehicle/HP-treated *Ido1* KO mice (Figure 3A). Similar results were achieved with administration of 200 mg/kg i.p. kynurenine and using normoxic vehicle-treated *Ido1* KO mice as controls (Figure S3B).

We next investigated whether an increase in serum kynurenine alone was sufficient to afford renoprotection under normoxia. Treatment of wild-type mice with an i.p. injection of kynurenine (200 mg/kg) 2 h prior to renal IRI led to a 1.5-fold reduction in *Vcam1* mRNA in post-ischemic kidneys of kynurenine-treated mice, but *Kim1* and *Tnfa* transcripts, injury scores, and Ly6.$B2^{+ve}$ infiltration were comparable to vehicle-treated mice (Figure 3B). While these findings suggest that an increase in serum kynurenine by exogenous administration is not sufficient to mimic HP, we also examined whether kynurenine administration enhances the renoprotection generated by PHI. For this purpose, animals were pretreated with a PHI (same as in Figure 2B, experimental protocol) and received either one single injection of kynurenine or normal saline 2 h prior to IRI. Based on the analysis of *Kim1*, *Vcam1*, and *Tnfa* mRNA, kynurenine administration failed to enhance the cytoprotection generated by PHD inhibition (Figure S3C). Because these findings suggest that an increase in serum kynurenine by exogenous administration is not sufficient to mimic or enhance the cytoprotective effects induced by activation of hypoxia signaling, the renoprotective action of kynurenine may require additional upstream hypoxia-induced alterations. In summary, our results demonstrate that the increase in serum kynurenine is required in the concerted molecular response by which HP provides protection against post-ischemic kidney injury and inflammation.

HP preserves NAD^+ levels in the post-ischemic kidney to promote favorable metabolic reprogramming

To understand how HP provides protection against post-ischemic renal injury, we performed RNA sequencing (RNA-seq) analysis on the post-IRI kidneys of wild-type mice subjected

cells/HPF. Bottom graphs show *Kim1*, *Vcam1*, and *Tnfa* mRNA in IR and contralateral kidneys. (A) For AKI score, n = 7 (Nx, IR) and 8 (Hx, IR); for Ly-6B.2^{+ve} cells/HPF, n = 4; for *Kim1* and *Tnfa* mRNA, n = 7 (Nx) and 8 (Hx); and for *Vcam1* mRNA, n = 6 (Nx) and 8 (Hx). (B) n = 4. Error bars represent SEM. For AKI scores and Ly-6B.2^{+ve} cell counts in (A) and (B), statistics were determined by two-tailed t test. All other comparisons were performed by one-way ANOVA with Sidak correction. *$p < 0.05$; ns, not statistically significant. uIRI, unilateral IRI; IR, kidney subjected to uIRI; CTL, contralateral kidney. Scale bar indicates 50 μm.

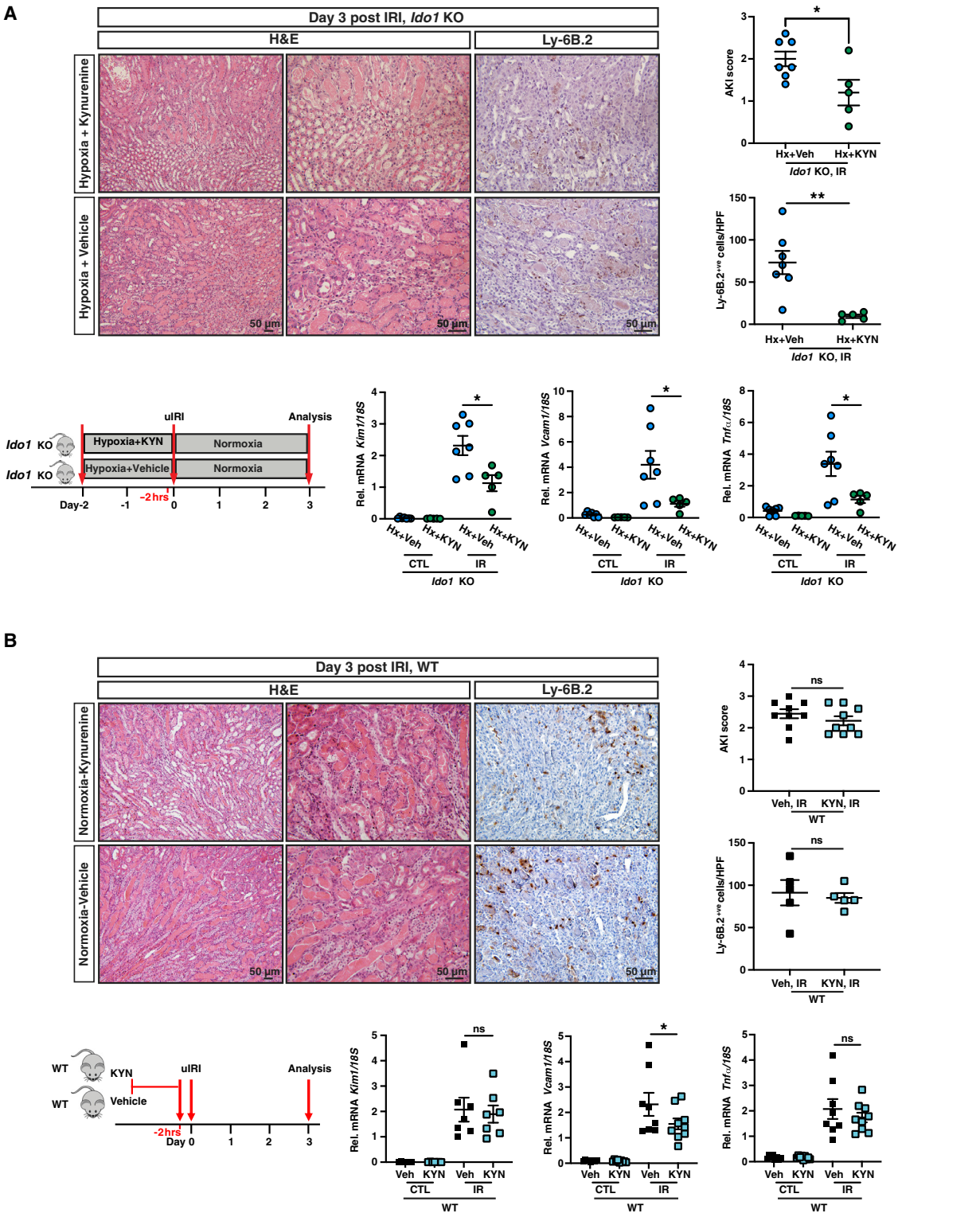

Figure 3. Exogenous administration of kynurenine is not sufficient to provide renoprotection under normoxia but restores the HP in the context of IDO1 deficiency

(A and B) Schematic of the experimental protocol, representative images of H&E- and Ly-6B.2-stained sections of day 3 post-IRI kidneys from *Ido1* KO mice subjected to HP and kynurenine administration (50 mg/kg) compared to HP/vehicle-treated *Ido1* KO mice (A) or WT mice treated with kynurenine (200 mg/kg) versus vehicle under normoxia (B). Right panels demonstrate scoring of tubular injury (A, n = 7 [Hx+Veh] and 5 [Hx+KYN]; B, n = 9) and quantification of Ly6B.2^{+ve}

(legend continued on next page)

to HP compared to normoxic controls. RNA-seq identified 2,633 differentially expressed genes (DEGs) in the context of HP, and heatmap of the top100 most DEGs showed a distinct transcriptional profile in HP compared to normoxia (Figure S4A). Following Gene Ontology (GO) term enrichment analysis, we detected immune system process and inflammatory response among the key pathways regulated by HP (Figure S4B). Consistent with the blunted inflammation by HP was the suppression of several genes encoding inflammatory molecules, including chemokine (C-C motif) ligand 2 (*Ccl2*), chemokine (C-X-C motif) ligand 2 (*Cxcl2*), and chitinase-like 3 (*Chil3*) (Figure 4A). On the other hand, among the upregulated genes, *Cxcl12* promotes kidney repair by facilitating glycolysis (Yakulov et al., 2018), while *Ccl28* has been implicated in dampening inflammation in hypoxic tumors by promoting the recruitment of regulatory T (Treg) cells (Facciabene et al., 2011).

KEGG pathway analysis of DEGs revealed significant enrichment in several metabolic and signaling pathways (Figure 4B). Remarkably, tryptophan metabolism was identified among the most enriched metabolic pathways in post-ischemic kidneys subjected to HP. To validate this finding, we quantified the transcripts encoding enzymes in the KP by RT-PCR. As shown in Figure 4C, we found significant upregulation of *Ido2*, kynurenine aminotransferase 3 (*Kyat3*), kynurenine 3-monooxygenase (*Kmo*), and kynureninase (*Kynu*) (Figure 4C). These findings motivated us to further investigate the impact of HP on generation of KP metabolites and NAD^+. We observed significant increases in KYNA (by 345%), XA (by 171%), 3-HAA (by 219%), QUIN (by 216%), and NAD^+ (by 35%) in post-IRI kidneys of HP-subjected mice compared to normoxic controls (Figure 4D). The increase in NAD^+ was also confirmed by a biochemical assay (Figure S4C). Importantly, the analysis of PHI-treated post-IRI kidneys yielded consistent results, with even more prominent increase in NAD^+ levels by 118% (Figure 4D). NAD^+ has emerged as a key metabolite exerting cytoprotection through an array of actions that include regulation of cellular metabolism and antioxidant defense (Cantó et al., 2015; Ralto et al., 2020). As shown in Figure 4E, we found significant upregulation of genes involved in ketone body metabolism, fatty acid oxidation, and glutathione metabolism, a coordinated metabolic response that may protect from bioenergetic failure in AKI. For instance, upregulation of glutathione metabolism related genes enhances antioxidant defense, while tissue ketogenesis has been implicated in the renoprotective effects mediated by SGLT2 inhibition (Tomita et al., 2020). Also, among the upregulated genes involved in fatty acid oxidation, peroxisome proliferator-activated receptor gamma coactivator 1-alpha (*Ppargc1a*) protects against tubular injury from diverse insults such as IRI, toxins, and sepsis (Kang et al., 2015; Tran et al., 2011, 2016). Of interest, skeletal muscle *Ppargc1a* ameliorates stress-induced depression by enhancing the conversion of kynurenine into kynurenic acid through induction of *Kyats* (Agudelo et al., 2014). Therefore, our data suggest that HP protects against ischemic kidney injury by increasing circulating kynurenine and boosting the generation of kynurenine metabolites and NAD^+ through activation of the KP in the post-ischemic kidney.

DISCUSSION

Besides their role in energy conversion, metabolites have a myriad of functions in dictating responses to cellular injury. Here, we show that two potent cytoprotective strategies, HP and pharmacologic inhibition of PHDs, lead to systemic accumulation of the tryptophan metabolite, kynurenine. The increase in serum kynurenine represents an essential metabolic adaptation in the context of renoprotection generated by both HP and PHD inhibition. Furthermore, by enhancing the kynurenine biotransformation in the post-ischemic kidney, HP generates kynurenine metabolites and NAD^+, a response that augments kidney tissue resilience against ischemic injury.

Our findings, together with recently published studies, suggest that the KP may be one of the key pathways mediating organ protection by HP. First, the fact that the KP emerged from non-biased metabolomic screening in our study and in the cardioprotection study by Olenchock et al. (2016) suggests that this metabolic pathway plays a central and perhaps unifying role in organ protection provided by HP. Second, kynurenine interacts with the arylhydrocarbon receptor (Ahr) with downstream effects that include, among others, induction of Treg cells (Mezrich et al., 2010) and inhibition of the nucleotide-binding domain, leucine-rich repeat, and pyrin domain containing protein 3 (*Nlrp3*) transcription and inflammasome activation (Huai et al., 2014), effects known to suppress post-ischemic inflammation (Anders and Muruve, 2011; Kinsey et al., 2009; Nazir et al., 2017). Consistently, we found downregulation of *Nlrp3* in wild-type mice subjected to HP, an effect that was lost in *Ido1* KO mice but could be restored upon injection of kynurenine (Figure S4D). Third, kynurenine is converted to other metabolites with immunosuppressant functions. Specifically, kynurenic acid reduces the inflammatory response triggered by lipopolysaccharide in macrophages (Tiszlavicz et al., 2011) and controls cytokine release from invariant natural killer T (iNKT) cells by interacting with G-protein-coupled receptor 35 (GPR35) (Fallarini et al., 2010). Other examples include 3-hydroxyanthranilic acid and quinolinic acid, which induce apoptosis of type 1 T helper (Th1) cells, while promoting proliferation of type 2 T helper (Th2) cells, a switch that protects against hyperinflammation (Fallarino et al., 2002). Finally, KP enzymes have been shown to play critical roles in preserving tissue homeostasis against injury and inflammation. Specifically, IDO1-driven activation of general control nonderepressible 2 (GCN2)-dependent signals induces autophagy and reduces inflammatory pathology in a mouse model of glomerulonephritis (Chaudhary et al., 2015). Similarly, IDO1 limits

cells/HPF (A, n = 7 [Hx+Veh] and 5 [Hx+KYN]; B, n = 5). Bottom graphs show *Kim1*, *Vcam1*, and *Tnfa* mRNA levels in IR and CTL kidneys (A, n = 7 [Hx+Veh] and 5 [Hx+KYN]; B, n = 7 for *Kim1*, n = 8 [Veh] and 9 [KYN] for *Vcam1* and *Tnfa*). Error bars represent SEM. For AKI scores and Ly-6B.2^{+ve} cell counts in (A) and (B), statistics were determined by two-tailed t test. All other comparisons were performed by one-way ANOVA with Sidak correction. *$p < 0.05$; **$p < 0.01$; ns, not statistically significant. Scale bar indicates 50 μm.

A

Inflammatory pathway genes	
Gene name	Log2FC
Adgre1	-1.91
Axl	-2.25
Csf1	-2.07
Lcn2	-3.26
Lgals9	-2.06
Ccl12	-3.51
Ccl2	-4.01
Ccl3	-5.59
Ccl6	-3.28
Ccl7	-4.02
Ccl9	-2.95
Chil3	-4.40
Cxcl2	-3.37
C1q	-2.88
Fga	+3.86
Ido2	+4.30
Ccl28	+4.19
Cxcl12	+1.61

B

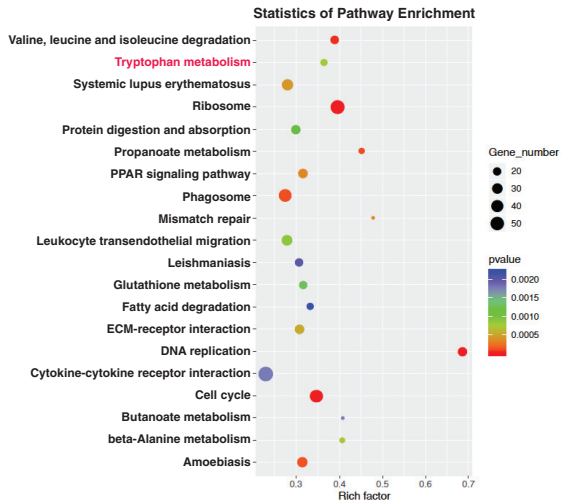

C

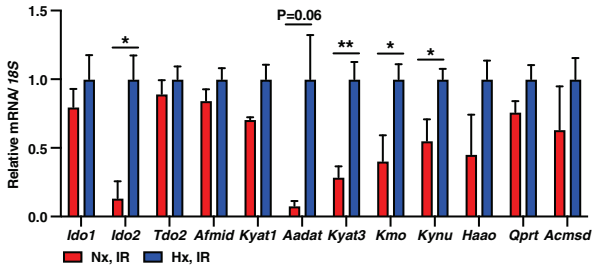

D

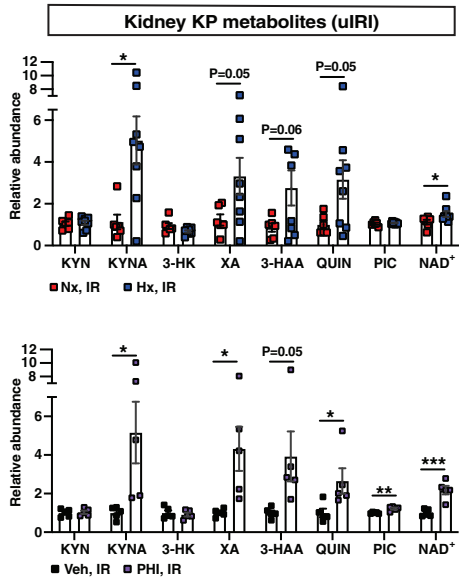

E

Metabolic pathway genes	
Gene name	Log2FC
Ketone Body Metabolism	
Hmgcs2	+4.42
Bdh1	+2.51
Aacs	+1.67
Acss3	+1.66
Fatty Acid Oxidation	
Hao2	+2.07
Acox2	+2.27
Acox3	+1.88
Ehhadh	+3.18
Crot	+1.97
Cd36	+2.01
Ppargc1a	+1.56
Glutathione metabolism	
Gclc	+1.78
Anpep	+1.63
Gpx3	+3.15
Gpx6	+3.80

Figure 4. HP suppresses proinflammatory pathways and preserves NAD$^+$ levels in the post-ischemic kidney to promote favorable metabolic reprogramming

(A) Shown is a list of selected genes with ontologies of inflammatory response and immune system process among DEGs in response to HP with a $\log_2$FC greater than 1 or less than −1 and false discovery rate (FDR)-adjusted $p < 0.05$.

(B) KEGG enrichment graph displays the top 20 pathways. The number of DEGs enriched in KEGG terms, p value, and rich factor are shown in scatterplot. Rich factor = (number of DEGs in KEGG term)/(total number of genes in KEGG term).

(C and D) Relative mRNA levels of genes associated with tryptophan metabolism (n = 3 [Nx, IR] and 4 [Hx, IR]) (C) and KP metabolites (D) in day 3 post-IRI kidneys from mice subjected to HP (upper panel) compared to normoxia (n = 6 [Nx, IR] and 8 [Hx, IR]) or PHI-treated mice compared to vehicle (n = 5) (lower panel).

(E) List of selected metabolic pathway genes among DEGs in response to HP with FDR-adjusted $p < 0.05$.

(legend continued on next page)

vascular inflammation and atherosclerosis in *ApoE*$^{-/-}$ mice (Cole et al., 2015; Polyzos et al., 2015). Furthermore, inhibition of kynurenine 3-monooxygenase (KMO), an intervention that raises serum kynurenine, protects against tissue injury in experimental multiorgan dysfunction syndrome (Mole et al., 2016).

NAD^+ has emerged as a guardian promoting renal resistance against insults by connecting oxidative metabolism in the epithelium to overall organ function. Augmentation of NAD^+ levels by increasing PGC1a levels (Kang et al., 2015; Tran et al., 2011, 2016), providing the precursor nicotinamide (Poyan Mehr et al., 2018), or α-amino-β-carboxymuconate-ε-semialdehyde decarboxylase (ACMSD) inhibition (Katsyuba et al., 2018) protects against AKI. Our study now demonstrates that HP increased circulating kynurenine and preserved NAD^+ levels following renal IRI, perhaps by promoting kynurenine degradation to NAD^+ in the post-ischemic kidney. Our findings have implications on the interpretation of two recent negative trials on ischemic preconditioning (Hausenloy et al., 2015; Meybohm et al., 2015). Defects in hypoxic response and tryptophan metabolism due to aging, comorbidities, and medications (Cho et al., 2021; Kartika et al., 2020; Orabona et al., 2018; Takabuchi et al., 2004) may have blunted the beneficial effects of remote ischemic preconditioning, issues that warrant further investigation.

Collectively, our findings indicate that HP and PHD inhibition increase circulating kynurenine, which functions as a critical metabolic signal in mediating renoprotection by these approaches. It could therefore represent a valuable target to protect against ischemic AKI and potentially synergize with emerging therapies focused on NAD^+ preservation.

LIMITATIONS OF STUDY

First, our study identified kynurenine as an essential metabolite in renoprotective responses generated by HP and PHI, but it cannot be assumed that it is the sole mediator. Second, while HP and PHI preserve NAD^+ levels in the post-ischemic kidney, probably through a combination of increased circulating kynurenine and induction of genes encoding enzymes in tryptophan metabolism, the exact pathway by which kynurenine acts on kidney tissue remains to be explored. Third, IDO1 is required for the increase in serum kynurenine observed following HP and PHD inhibition, but it remains unclear which cells drive this response and how alterations in other enzymatic steps contribute. Finally, it remains to be determined whether the systemic alteration in tryptophan metabolism represents a broader mechanism for homeostatic regulation in the context of hypoxia.

STAR★METHODS

Detailed methods are provided in the online version of this paper and include the following:

SUPPLEMENTAL INFORMATION

Supplemental information can be found online at https://doi.org/10.1016/j.celrep.2021.109547.

ACKNOWLEDGMENTS

This work was supported by National Institutes of Health (NIH) grants P20 GM104936 (P.P.K.), R01DK115850 (P.P.K.), R35GM119528 (R.L.), T32DK071496 (R. Torosyan). Metabolomics services were performed by the Metabolomics Core Facility at Robert H. Lurie Comprehensive Cancer Center of Northwestern University. We acknowledge the Northwestern University George M. O'Brien Kidney Research Core Center (NU GoKidney), an NIH/NIDDK-funded program (P30 DK114857), for their core services and support. We thank Breeanna Mintmier (West Virginia University) for performing LC/UV-based quantification of serum kynurenine. The funders had no role in study design, data collection and interpretation, or the decision to submit the work for publication.

AUTHOR CONTRIBUTIONS

P.P.K. and R. Torosyan conceived the study; S.H., R. Torosyan, P.V.B., and P.P.K. designed the experiments; S.H., R. Torosyan, R. Tiwari, S.A., M.P.S., G.R., M.K., B.G., E.W.K., and P.P.K. performed experiments; S.H., R. Torosyan, P.V.B., R. Tiwari, S.A., M.P.S., G.R., M.K., B.G., A.T., S.B., E.W.K., R.L., P.G., N.S.D., and P.P.K. analyzed and interpreted data; M.W.C. developed and optimized the quantitative LC/MS assay for measurement of kynurenine and tryptophan; E.W.K. and R.L. developed and optimized the LC/UV-based assay for quantification of kynurenine; P.G. developed and optimized the HPLC-MS/MS assay for measurement of KP metabolites; P.P.K. wrote the manuscript; and all authors approved and commented on the manuscript.

Error bars represent SEM. For (C) and (D), statistics were determined by two-tailed t test; *p < 0.05. *Afmid*, arylformamidase; *Kyat*, kynurenine aminotransferase; *Aadat*, aminoadipate aminotransferase; *Kmo*, kynurenine 3-monooxygenase; *Kynu*, kynurerinase; *Haao*, 3-hydroxyanthranilate 3,4-dioxygenase; *Qprt*, quinolinate phosphoribosyltransferase; *Acmsd*, alpha-amino-beta-carboxy-muconate-semialdehyde decarboxylase. KYN, kynurenine; KYNA, kynurenic acid; 3-HK, 3-hydroxykynurenine; XA, xanthurenic acid; 3-HAA, 3-hydroxyanthranilic acid; QUIN; quinolinic acid, PIC; picolinic acid.

DECLARATION OF INTERESTS

The authors declare no competing interests.

Received: September 10, 2020
Revised: May 6, 2021
Accepted: July 27, 2021
Published: August 17, 2021

REFERENCES

Agudelo, L.Z., Femenía, T., Orhan, F., Porsmyr-Palmertz, M., Goiny, M., Martinez-Redondo, V., Correia, J.C., Izadi, M., Bhat, M., Schuppe-Koistinen, I., et al. (2014). Skeletal muscle PGC-1α1 modulates kynurenine metabolism and mediates resilience to stress-induced depression. Cell *159*, 33–45.

Anders, H.-J., and Muruve, D.A. (2011). The inflammasomes in kidney disease. J. Am. Soc. Nephrol. *22*, 1007–1018.

Baban, B., Chandler, P., McCool, D., Marshall, B., Munn, D.H., and Mellor, A.L. (2004). Indoleamine 2,3-dioxygenase expression is restricted to fetal trophoblast giant cells during murine gestation and is maternal genome specific. J. Reprod. Immunol. *61*, 67–77.

Bernhardt, W.M., Câmpean, V., Kany, S., Jürgensen, J.S., Weidemann, A., Warnecke, C., Arend, M., Klaus, S., Günzler, V., Amann, K., et al. (2006). Preconditional activation of hypoxia-inducible factors ameliorates ischemic acute renal failure. J. Am. Soc. Nephrol. *17*, 1970–1978.

Cantó, C., Menzies, K.J., and Auwerx, J. (2015). NAD(+) Metabolism and the Control of Energy Homeostasis: A Balancing Act between Mitochondria and the Nucleus. Cell Metab. *22*, 31–53.

Cervenka, I., Agudelo, L.Z., and Ruas, J.L. (2017). Kynurenines: Tryptophan's metabolites in exercise, inflammation, and mental health. Science *357*, eaaf9794.

Chaudhary, K., Shinde, R., Liu, H., Gnana-Prakasam, J.P., Veeranan-Karmegam, R., Huang, L., Ravishankar, B., Bradley, J., Kvirkvelia, N., McMenamin, M., et al. (2015). Amino acid metabolism inhibits antibody-driven kidney injury by inducing autophagy. J. Immunol. *194*, 5713–5724.

Cho, S.J., Hong, K.S., Schenck, E., Lee, S., Harris, R., Yang, J., Choi, A.M.K., and Stout-Delgado, H. (2021). Decreased IDO1-dependent tryptophan metabolism in aged lung during influenza. Eur. Respir. J. *57*, 2000443.

Cole, J.E., Astola, N., Cribbs, A.P., Goddard, M.E., Park, I., Green, P., Davies, A.H., Williams, R.O., Feldmann, M., and Monaco, C. (2015). Indoleamine 2,3-dioxygenase-1 is protective in atherosclerosis and its metabolites provide new opportunities for drug development. Proc. Natl. Acad. Sci. USA *112*, 13033–13038.

Eltzschig, H.K., Bratton, D.L., and Colgan, S.P. (2014). Targeting hypoxia signalling for the treatment of ischaemic and inflammatory diseases. Nat. Rev. Drug Discov. *13*, 852–869.

Epstein, A.C.R., Gleadle, J.M., McNeill, L.A., Hewitson, K.S., O'Rourke, J., Mole, D.R., Mukherji, M., Metzen, E., Wilson, M.I., Dhanda, A., et al. (2001). C. elegans EGL-9 and mammalian homologs define a family of dioxygenases that regulate HIF by prolyl hydroxylation. Cell *107*, 43–54.

Facciabene, A., Peng, X., Hagemann, I.S., Balint, K., Barchetti, A., Wang, L.-P., Gimotty, P.A., Gilks, C.B., Lal, P., Zhang, L., and Coukos, G. (2011). Tumour hypoxia promotes tolerance and angiogenesis via CCL28 and T(reg) cells. Nature *475*, 226–230.

Fallarini, S., Magliulo, L., Paoletti, T., de Lalla, C., and Lombardi, G. (2010). Expression of functional GPR35 in human iNKT cells. Biochem. Biophys. Res. Commun. *398*, 420–425.

Fallarino, F., Grohmann, U., Vacca, C., Bianchi, R., Orabona, C., Spreca, A., Fioretti, M.C., and Puccetti, P. (2002). T cell apoptosis by tryptophan catabolism. Cell Death Differ. *9*, 1069–1077.

Hausenloy, D.J., Candilio, L., Evans, R., Ariti, C., Jenkins, D.P., Kolvekar, S., Knight, R., Kunst, G., Laing, C., Nicholas, J., et al.; ERICCA Trial Investigators (2015). Remote Ischemic Preconditioning and Outcomes of Cardiac Surgery. N. Engl. J. Med. *373*, 1408–1417.

Hill, P., Shukla, D., Tran, M.G.B., Aragones, J., Cook, H.T., Carmeliet, P., and Maxwell, P.H. (2008). Inhibition of hypoxia inducible factor hydroxylases protects against renal ischemia-reperfusion injury. J. Am. Soc. Nephrol. *19*, 39–46.

Huai, W., Zhao, R., Song, H., Zhao, J., Zhang, L., Zhang, L., Gao, C., Han, L., and Zhao, W. (2014). Aryl hydrocarbon receptor negatively regulates NLRP3 inflammasome activity by inhibiting NLRP3 transcription. Nat. Commun. *5*, 4738.

Johnsen, M., Kubacki, T., Yeroslaviz, A., Späth, M.R., Mörsdorf, J., Göbel, H., Bohl, K., Ignarski, M., Meharg, C., Habermann, B., et al. (2020). The Integrated RNA Landscape of Renal Preconditioning against Ischemia-Reperfusion Injury. J. Am. Soc. Nephrol. *31*, 716–730.

Kang, H.M., Ahn, S.H., Choi, P., Ko, Y.-A., Han, S.H., Chinga, F., Park, A.S.D., Tao, J., Sharma, K., Pullman, J., et al. (2015). Defective fatty acid oxidation in renal tubular epithelial cells has a key role in kidney fibrosis development. Nat. Med. *21*, 37–46.

Kapitsinou, P.P., and Haase, V.H. (2015). Molecular mechanisms of ischemic preconditioning in the kidney. Am. J. Physiol. Renal Physiol. *309*, F821–F834.

Kapitsinou, P.P., Jaffe, J., Michael, M., Swan, C.E., Duffy, K.J., Erickson-Miller, C.L., and Haase, V.H. (2012). Preischemic targeting of HIF prolyl hydroxylation inhibits fibrosis associated with acute kidney injury. Am. J. Physiol. Renal Physiol. *302*, F1172–F1179.

Kapitsinou, P.P., Sano, H., Michael, M., Kobayashi, H., Davidoff, O., Bian, A., Yao, B., Zhang, M.Z., Harris, R.C., Duffy, K.J., et al. (2014). Endothelial HIF-2 mediates protection and recovery from ischemic kidney injury. J. Clin. Invest. *124*, 2396–2409.

Kapitsinou, P.P., Rajendran, G., Astleford, L., Michael, M., Schonfeld, M.P., Fields, T., Shay, S., French, J.L., West, J., and Haase, V.H. (2016). The Endothelial Prolyl-4-Hydroxylase Domain 2/Hypoxia-Inducible Factor 2 Axis Regulates Pulmonary Artery Pressure in Mice. Mol. Cell. Biol. *36*, 1584–1594.

Kartika, R., Wibowo, H., Purnamasari, D., Pradipta, S., and Larasati, R.A. (2020). Altered Indoleamine 2,3-Dioxygenase Production and Its Association to Inflammatory Cytokines in Peripheral Blood Mononuclear Cells Culture of Type 2 Diabetes Mellitus. Int. J. Tryptophan Res. *13*, 1178646920978236.

Katsyuba, E., Mottis, A., Zietak, M., De Franco, F., van der Velpen, V., Gariani, K., Ryu, D., Cialabrini, L., Matilainen, O., Liscio, P., et al. (2018). De novo NAD^+ synthesis enhances mitochondrial function and improves health. Nature *563*, 354–359.

Kim, D., Langmead, B., and Salzberg, S.L. (2015). HISAT: a fast spliced aligner with low memory requirements. Nat. Methods *12*, 357–360.

Kinsey, G.R., Sharma, R., Huang, L., Li, L., Vergis, A.L., Ye, H., Ju, S.-T., and Okusa, M.D. (2009). Regulatory T cells suppress innate immunity in kidney ischemia-reperfusion injury. J. Am. Soc. Nephrol. *20*, 1744–1753.

Majmundar, A.J., Wong, W.J., and Simon, M.C. (2010). Hypoxia-inducible factors and the response to hypoxic stress. Mol. Cell *40*, 294–309.

Martin, M. (2011). Cutadapt removes adapter sequences from high-throughput sequencing reads. EMBnet. J. *17*, 3.

Meybohm, P., Bein, B., Brosteanu, O., Cremer, J., Gruenewald, M., Stoppe, C., Coburn, M., Schaelte, G., Böning, A., Niemann, B., et al.; RIPHeart Study Collaborators (2015). A Multicenter Trial of Remote Ischemic Preconditioning for Heart Surgery. N. Engl. J. Med. *373*, 1397–1407.

Mezrich, J.D., Fechner, J.H., Zhang, X., Johnson, B.P., Burlingham, W.J., and Bradfield, C.A. (2010). An interaction between kynurenine and the aryl hydrocarbon receptor can generate regulatory T cells. J. Immunol. *185*, 3190–3198.

Mole, D.J., Webster, S.P., Uings, I., Zheng, X., Binnie, M., Wilson, K., Hutchinson, J.P., Mirguet, O., Walker, A., Beaufils, B., et al. (2016). Kynurenine-3-monooxygenase inhibition prevents multiple organ failure in rodent models of acute pancreatitis. Nat. Med. *22*, 202–209.

Murry, C.E., Jennings, R.B., and Reimer, K.A. (1986). Preconditioning with ischemia: a delay of lethal cell injury in ischemic myocardium. Circulation *74*, 1124–1136.

Nazir, S., Gadi, I., Al-Dabet, M.M., Elwakiel, A., Kohli, S., Ghosh, S., Manoharan, J., Ranjan, S., Bock, F., Braun-Dullaeus, R.C., et al. (2017).

Cytoprotective activated protein C averts Nlrp3 inflammasome-induced ischemia-reperfusion injury via mTORC1 inhibition. Blood *130*, 2664–2677.

Olenchock, B.A., Moslehi, J., Baik, A.H., Davidson, S.M., Williams, J., Gibson, W.J., Chakraborty, A.A., Pierce, K.A., Miller, C.M., Hanse, E.A., et al. (2016). EGLN1 Inhibition and Rerouting of α-Ketoglutarate Suffice for Remote Ischemic Protection. Cell *164*, 884–895.

Orabona, C., Mondanelli, G., Pallotta, M.T., Carvalho, A., Albini, E., Fallarino, F., Vacca, C., Volpi, C., Belladonna, M.L., Berioli, M.G., et al. (2018). Deficiency of immunoregulatory indoleamine 2,3-dioxygenase 1in juvenile diabetes. JCI Insight *3*, e96244.

Pertea, M., Pertea, G.M., Antonescu, C.M., Chang, T.-C., Mendell, J.T., and Salzberg, S.L. (2015). StringTie enables improved reconstruction of a transcriptome from RNA-seq reads. Nat. Biotechnol. *33*, 290–295.

Polyzos, K.A., Ovchinnikova, O., Berg, M., Baumgartner, R., Agardh, H., Pirault, J., Gisterå, A., Assinger, A., Laguna-Fernandez, A., Bäck, M., et al. (2015). Inhibition of indoleamine 2,3-dioxygenase promotes vascular inflammation and increases atherosclerosis in Apoe-/- mice. Cardiovasc. Res. *106*, 295–302.

Poyan Mehr, A., Tran, M.T., Ralto, K.M., Leaf, D.E., Washco, V., Messmer, J., Lerner, A., Kher, A., Kim, S.H., Khoury, C.C., et al. (2018). De novo NAD^+ biosynthetic impairment in acute kidney injury in humans. Nat. Med. *24*, 1351–1359.

Ralto, K.M., Rhee, E.P., and Parikh, S.M. (2020). NAD^+ homeostasis in renal health and disease. Nat. Rev. Nephrol. *16*, 99–111.

Robinson, M.D., McCarthy, D.J., and Smyth, G.K. (2010). edgeR: a Bioconductor package for differential expression analysis of digital gene expression data. Bioinformatics *26*, 139–140.

Schofield, C.J., and Ratcliffe, P.J. (2004). Oxygen sensing by HIF hydroxylases. Nat. Rev. Mol. Cell Biol. *5*, 343–354.

Semenza, G.L. (2012). Hypoxia-inducible factors in physiology and medicine. Cell *148*, 399–408.

Takabuchi, S., Hirota, K., Nishi, K., Oda, S., Oda, T., Shingu, K., Takabayashi, A., Adachi, T., Semenza, G.L., and Fukuda, K. (2004). The intravenous anesthetic propofol inhibits hypoxia-inducible factor 1 activity in an oxygen tension-dependent manner. FEBS Lett. *577*, 434–438.

Tiszlavicz, Z., Németh, B., Fülöp, F., Vécsei, L., Tápai, K., Ocsovszky, I., and Mándi, Y. (2011). Different inhibitory effects of kynurenic acid and a novel kynurenic acid analogue on tumour necrosis factor-α (TNF-α) production by mononuclear cells, HMGB1 production by monocytes and HNP1-3 secretion by neutrophils. Naunyn Schmiedebergs Arch. Pharmacol. *383*, 447–455.

Tomita, I., Kume, S., Sugahara, S., Osawa, N., Yamahara, K., Yasuda-Yamahara, M., Takeda, N., Chin-Kanasaki, M., Kaneko, T., Mayoux, E., et al. (2020). SGLT2 Inhibition Mediates Protection from Diabetic Kidney Disease by Promoting Ketone Body-Induced mTORC1 Inhibition. Cell Metab. *32*, 404–419.

Tran, M., Tam, D., Bardia, A., Bhasin, M., Rowe, G.C., Kher, A., Zsengeller, Z.K., Akhavan-Sharif, M.R., Khankin, E.V., Saintgeniez, M., et al. (2011). PGC-1α promotes recovery after acute kidney injury during systemic inflammation in mice. J. Clin. Invest. *121*, 4003–4014.

Tran, M.T., Zsengeller, Z.K., Berg, A.H., Khankin, E.V., Bhasin, M.K., Kim, W., Clish, C.B., Stillman, I.E., Karumanchi, S.A., Rhee, E.P., and Parikh, S.M. (2016). PGC1α drives NAD biosynthesis linking oxidative metabolism to renal protection. Nature *531*, 528–532.

Veres, G., Molnár, M., Zádori, D., Szentirmai, M., Szalárdy, L., Török, R., Fazekas, E., Ilisz, I., Vécsei, L., and Klivényi, P. (2015). Central nervous system-specific alterations in the tryptophan metabolism in the 3-nitropropionic acid model of Huntington's disease. Pharmacol. Biochem. Behav. *132*, 115–124.

Yakulov, T.A., Todkar, A.P., Slanchev, K., Wiegel, J., Bona, A., Groß, M., Scholz, A., Hess, I., Wurditsch, A., Grahammer, F., et al. (2018). CXCL12 and MYC control energy metabolism to support adaptive responses after kidney injury. Nat. Commun. *9*, 3660.

STAR★METHODS

KEY RESOURCES TABLE

REAGENT or RESOURCE	SOURCE	IDENTIFIER
Antibodies		
Rat monoclonal anti Mouse Ly-6B.2	Bio-rad	Cat#MCA771G; RRID: AB_322950
Chemicals, peptides, and recombinant proteins		
IOX 2	Tocris	Cat# 4451
L-Kynurenine	Sigma-Aldrich	Cat#K8625
L-Tryptophan	Sigma-Aldrich	Cat#T0254
Water, BAKER ANALYZED LC/MS Reagent Grade	J.T. Baker	Cat#9831-02
Methylcellulose	ACROS Organics	182311000
TRIzol™ reagent	Invitrogen	Cat#15596026
High Capacity cDNA Reverse Transcription Kit	Applied Biosystems	Cat# 4368814
Power SYBR Green PCR Master Mix	Applied Biosystems	Cat#4368706
TaqMan Universal PCR Master Mix	Applied Biosystems	Cat#4305719
Critical commercial assays		
NAD/NADH Assay	Biovision	Cat#K337
Mouse EPO Quantakine ELISA Kit	R&D systems	Cat#MEP00B
Standard for Tryptophan-d5	Cambridge Isotope Laboratories	Cat#DLM-1092-PK
Standard for Kynurenine-d4	Cambridge Isotope Laboratories	Cat#DLM-7842-PK
3-Nitro-L-tyrosine	Sigma-Aldrich	Cat#851914
2-propanolol (LC-MS)	MilliporeSigma	Cat#1027814000
Acetonitrile (LC-MS)	MilliporeSigma	Cat# 1000294000
Bio-Rad Protein Assay	BioRad	Cat# 5000001
Deposited data		
RNaseq data	This manuscript-GEO	GEO: GSE156516
Metabolomic data	This data has been deposited at the NIH Common Fund's NMDR website, https://www.metabolomicsworkbench.org	Project id PR001178; https://doi.org/10.21228/M8F99F
Experimental models: Organisms/strains		
Mus musculus (C57BL/6J)	The Jackson Laboratory	stock#000664
Mus musculus Ido1 KO	The Jackson Laboratory	stock#005867
Oligonucleotides		
Ido1 Mutant Forward 5′-CGTGCAATCCATCTTGTTCA-3′	Integrated DNA Technologies	N/A
Ido1 Wild type Forward 5′-TATTGAAAGGGGAATCCAGA −3′	Integrated DNA Technologies	N/A
Ido1 Reverse 5′- GTGTCAGAAAGCTCACTGCTT −3′	Integrated DNA Technologies	N/A
RT-PCR *Tnfα* forward 5′-GCTGAGCTCAAACCCTGGTA-3′	Integrated DNA Technologies	N/A
RT-PCR *Tnfα* reverse 5′-CGGACTCCGCAAAGTCTAAG-3′	Integrated DNA Technologies	N/A
RT-PCR *Vcam1* forward 5′- TAGAGTGCAAGGAGTTCGGG −3′	Integrated DNA Technologies	N/A
RT-PCR *Vcam1* reverse 5′-CCGGCATATACGAGTGTGAA-3′	Integrated DNA Technologies	N/A
RT-PCR *Kim1* forward 5′-AAACCAGAGATTCCCACACG-3′	Integrated DNA Technologies	N/A
RT-PCR *Kim1* reverse 5′-GTCGTGGGTCTTCCTGTAGC-3′	Integrated DNA Technologies	N/A
RT-PCR *Ido1* forward 5′-ACTGTGTCCTGGCAAACTGGAAG-3′	Integrated DNA Technologies	N/A
RT-PCR *Ido1* reverse 5′-AAGCTGCGATTTCCACCAATAGAG-3′	Integrated DNA Technologies	N/A
RT-PCR *Ido2* forward 5′-CTTGGCCCAAATGCATGATT-3′	Integrated DNA Technologies	N/A
RT-PCR *Ido2* reverse 5′-AAGATCCGGATGACCGAGTAAA-3′	Integrated DNA Technologies	N/A

(*Continued on next page*)

Continued

REAGENT or RESOURCE	SOURCE	IDENTIFIER
RT-PCR *Tdo2* forward 5′-GGCAGAGTTCCGGAAGCA-3′	Integrated DNA Technologies	N/A
RT-PCR *Tdo2* reverse 5′-CATGACGCTTCTCATCAAACAAG-3′	Integrated DNA Technologies	N/A
RT-PCR *Afmid* forward 5′-CCAGCAGATGGGTCATCCA-3′	Integrated DNA Technologies	N/A
RT-PCR *Afmid* reverse 5′-TCTGCACGAAGTTCCCAACA-3′	Integrated DNA Technologies	N/A
RT-PCR *Kmo* forward 5′-AGCTGAGCGAGGGAAGAATCT-3	Integrated DNA Technologies	N/A
RT-PCR *Kmo* reverse 5′-CAGCCCAAGCACGCAAAC-3′	Integrated DNA Technologies	N/A
RT-PCR *Kynu* forward 5′-GAAGTAATCGAGGAGGAAGGAGACT-3′	Integrated DNA Technologies	N/A
RT-PCR *Kynu* reverse 5′-AGTATAAAAGTGCAGCCCACTGAA-3′	Integrated DNA Technologies	N/A
RT-PCR *Haao* forward 5′- ACATCCCTAAGCCTGTTTGG −3′	Integrated DNA Technologies	N/A
RT-PCR *Haao* reverse 5′- CTATACACTGCCCTCCCATTG −3′	Integrated DNA Technologies	N/A
RT-PCR *Kyat1* forward 5′-AGCGCGTCCCTTTCCATAC-3′	Integrated DNA Technologies	N/A
RT-PCR *Kyat1* reverse 5′-GCGGAGACCTAAGAAGCGG-3′	Integrated DNA Technologies	N/A
RT-PCR *Aadat* forward 5′-ATGAATTACTCACGGTTCCTCAC-3′	Integrated DNA Technologies	N/A
RT-PCR *Aadat* reverse 5′-AACATGCTCGGGTTTGGAGAT-3′	Integrated DNA Technologies	N/A
RT-PCR *Kyat3* forward 5′-TTCAAAAACGCCAAACGAATCG-3′	Integrated DNA Technologies	N/A
RT-PCR *Kyat3* reverse 5′-GATGACCAAAGCCTCTTGTGT-3′	Integrated DNA Technologies	N/A
RT-PCR *Nlrp3* forward 5′-ATTACCCGCCCGAGAAAGG-3′	Integrated DNA Technologies	N/A
RT-PCR *Nlrp3* reverse 5′-TCGCAGCAAAGATCCACACAG-3′	Integrated DNA Technologies	N/A
RT-PCR *Qprt* forward 5′-CCGGTTCTAAAGCCGAAGAA-3′	Integrated DNA Technologies	N/A
RT-PCR *Qprt* reverse 5′-GCCCAACAAGCCGCAGTA-3′	Integrated DNA Technologies	N/A
RT-PCR *Acmsd* forward 5′-TCCACACTCATATTCTACCAAAGG-3′	Integrated DNA Technologies	N/A
RT-PCR *Acmsd* reverse 5′-AGCAGTTCTGTTGGATCACTC-3′	Integrated DNA Technologies	N/A
RT-PCR *Epo* forward 5′-CATCTGCGACAGTCGAGTTCTG-3′	Integrated DNA Technologies	N/A
RT-PCR *Epo* reverse 5′-CACAACCCATCGTGACATTTTC-3′	Integrated DNA Technologies	N/A
Software and algorithms		
Prism	Graphpad	https://www.graphpad.com/scientific-software/prism/
ImageJ	NIH	https://imagej.nih.gov/ij
FastQC	Babraham Bioinformatics	https://www.bioinformatics.babraham.ac.uk/projects/fastqc/
Adobe Illustrator	Adobe	https://www.adobe.com/products/illustrator.html
edgeR	Bioconductor	http://bioconductor.org/packages/release/bioc/html/edgeR.html
Xcalibur 4.1	Thermo Fisher Scientific	https://assets.thermofisher.com/TFS-Assets/CMD/manuals/man-xcali-97928-xcalibur-41-quan-start-manxcali97928-en.pdf
TraceFinder 4.1	Thermo Fisher Scientific	https://www.thermofisher.com/us/en/home/industrial/mass-spectrometry/liquid-chromatography-mass-spectrometry-lc-ms/lc-ms-software/lc-ms-data-acquisition-software/tracefinder-software.html
Other		
Amicon Ultra-0.5 Centrifugal Filter Unit	Millipore	UFC501024

RESOURCE AVAILABILITY

Lead contact

Further information and requests for resources and reagents should be directed to and will be fulfilled by the lead contact, Pinelopi P. Kapitsinou (pinelopi.kapitsinou@northwestern.edu)

Materials availability

This study did not generate new unique reagents.

Data and code availability

- The RNA-seq generated during this study are available on GEO: GSE156516. The metabolomic data has been deposited at the NIH Common Fund's NMDR (supported by NIH grant, U01-DK097430) website, the Metabolomics Workbench, https://www.metabolomicsworkbench.org where it has been assigned Project ID PR001178. The data can be accessed directly via the associated DOI: 10.21228/M8F99F.
- This paper does not report original code.
- Any additional information required to reanalyze the data reported in this paper is available from the lead contact upon request.

EXPERIMENTAL MODEL AND SUBJECT DETAILS

Mice

C57BL/6J mice (WT) and *Ido1* KO mice (stock#005867, C57BL/6J background) were purchased from the Jackson Laboratory (Bar Harbor, ME) and then bred in the Laboratory Research Animal Center of University of Kansas Medical Center. Mice were maintained in a specific pathogen-free facility on a 12-hour light/12-hour dark cycle. Littermates were randomly assigned to experimental groups.

Animal experiments

For the unilateral renal IRI model, anesthesia was induced with xylazine (10 mg/kg i.p.) and ketamine (90–120 mg/kg i.p.). After making a small midline abdominal incision, the left renal pedicle was occluded with a microaneurysm clamp while the right kidney was used as an internal control. The abdomen was partially closed, temporarily, with sutures, and body temperature was monitored by rectal probe and controlled with a heating pad at 37°C. After 25 minutes, the clamp was removed, and reperfusion was visually confirmed. The abdomen was closed with a 6-0 suture and the skin was closed with Michel miniature clips. Male mice 8-12 weeks of age were used for the renal IRI studies. For HP, mice were subjected to 8% O_2 in an animal hypoxia chamber (Biospherix Ltd) for 2 days prior to IRI. For pharmacologic PHD inhibition, HIF prolyl-4-hydroxylase inhibitor IOX2 (Tocris) was dissolved in 1% methylcellulose and administered by oral gavage at a dose of 60 mg/kg. Mice received a total of 2 doses of IOX2 6 hours and 2 days prior to IRI. Mice in the control group were treated with 1% methylcellulose (vehicle) at the same time points prior to IRI. For the kynurenine repletion experiments, mice were i.p. injected with L-kynurenine (50 mg.kg or 200 mg/kg) or normal saline 2hrs prior to renal IRI.

Study Approval

All animal studies were conducted in accordance with NIH guidelines for the use and care of live animal and were approved by the Institutional Animal Care and Use Committees at University of Kansas and at Northwestern University.

METHOD DETAILS

Histology

For the morphologic analysis, kidneys were fixed with 10% buffered formalin. Tubular injury was semiquantitatively graded based on the percentage of affected tubules (0, unaffected; 1, 1%–25%; 2, 26%–50%; 3, 51%–75%; 4, 76%–100%) in at least 5 random high-power fields in each section. Neutrophil infiltration was examined with a rat anti–Ly-6B.2 antibody (Bio-Rad, Hercules, CA), and for quantification, five random visual fields were analyzed per kidney section at a magnification of 200x using ImageJ software.

RNA isolation and Real-Time PCR

Total RNA was extracted with Trizol reagent (Invitrogen) according to the manufacturer's instructions. First-strand cDNA synthesis was performed with 1 μg of RNA using a High Capacity cDNA Reverse Transcription Kit (Applied BioSystems). For real-time PCR analysis, cDNA was subjected to PCR amplification using either SYBR Green PCR Master Mix or TaqMan Universal PCR Master Mix on the Step-One Plus Real-Time PCR system (Applied Biosystems). The sequences of the primers used in this study are reported in Table S1. 18S rRNA was used to normalize mRNA.

RNA sequencing

RNA integrity was checked with Agilent Technologies 2100 Bioanalyzer. Poly(A) RNA sequencing library was prepared by LC Sciences following Illumina's TruSeq-stranded-mRNA sample preparation protocol. Quality control analysis and quantification of the sequencing library were performed using Agilent Technologies 2100 Bioanalyzer High Sensitivity DNA Chip. Paired-ended sequencing was performed on Illumina's NovaSeq 6000 sequencing system. First, Cutadapt (Martin, 2011) and perl scripts in house were used to remove the reads that contained adaptor contamination, low quality bases and undetermined bases. Then sequence quality was verified using FastQC (https://www.bioinformatics.babraham.ac.uk/projects/fastqc/). HISAT2 (Kim et al., 2015) was used to map reads to the genome of ftp://ftp.ensembl.org/pub/release-96/fasta/mus_musculus/dna/. The mapped reads of each sample were assembled using StringTie (Pertea et al., 2015). Then, all transcriptomes were merged to reconstruct a comprehensive transcriptome using a proprietary Perl script of LC Sciences (Houston, Texas, USA). After the final transcriptome was generated, FPKM reads were evaluated by StringTie, and differential expressed genes were evaluated by edgeR (Robinson et al., 2010). The differentially expressed mRNAs and genes were selected with log2 (fold change) ≥ 1 or log2 (fold change) ≤ -1, and with p values < 0.05.

Metabolomic profiling

The metabolomic screening was conducted by Metabolon, Inc (Durham, NC). The sample preparation process was carried out using the automated MicroLab STAR® system from Hamilton Company. Sample preparation was conducted using a proprietary series of organic and aqueous extractions to remove the protein fraction while allowing maximum recovery of small molecules. The resulting extract was divided into two fractions; one for analysis by LC and one for analysis by GC. Samples were placed briefly on a TurboVap® (Zymark) to remove the organic solvent. Each sample was then frozen and dried under vacuum. Samples were then prepared for the appropriate instrument, either LC/MS or GC/MS.

Technical replicate samples created from a homogeneous pool containing a small amount of all study samples ("Client Matrix") were also included. The instrument variability was determined by calculating the median relative standard deviation for the internal standards that were added to each sample prior to injection into the mass spectrometers. The overall process variability was determined by calculating the median relative standard deviation for all endogenous metabolites present in 100% of the Client Matrix samples, which were technical replicates of pooled client samples.

The informatics system consisted of four major components, the Laboratory Information Management System (LIMS), the data extraction and peak-identification software, data processing tools for QC and compound identification, and a collection of information interpretation and visualization tools for use by data analysts. The hardware and software foundations for these informatics components were the LAN backbone, and a database server running Oracle 10.2.0.1 Enterprise Edition.

The data extraction of the raw mass spec data files yielded information that could be loaded into a relational database and manipulated without resorting to BLOB manipulation. Once in the database, the information was examined and appropriate QC limits were imposed. Peaks were identified using Metabolon's proprietary peak integration software, and component parts were stored in a separate, specifically designed complex data structure.

Compounds were identified by comparison to library entries of purified standards or recurrent unknown entities. Identification of known chemical entities was based on comparison to metabolomic library entries of purified standards. At the time of analysis, more than 1000 commercially available purified standard compounds had been acquired and registered into LIMS for distribution to both the LC and GC platforms for determination of their analytical characteristics. The combination of chromatographic properties and mass spectra gave an indication of a match to the specific compound or an isobaric entity.

LC-MS/MS-based quantification of kynurenine and tryptophan

Instrumentation

Sample analyses were carried out using a Waters Acquity UPLC system (Waters, Milford, MA), made up of a binary solvent manager, refrigerated sample manager, and a heated column manager. Tandem mass spectrometric detection was performed using a TSQ Quantum triple-stage quadrupole mass spectrometer (Thermo-Electron, San Jose, CA) equipped with a standard API-1 electrospray source and a 50 μm I.D. stainless steel capillary

Liquid chromatographic conditions

A BEH-C18 *Acquity* UPLC column (2.1 mm x 100 mm, 1.7 μm) (Waters, Milford MA) equipped with an Acquity UPLC in-line stainless steel filter unit (0.2 μm, Waters) was used for all chromatographic separations. The column and autosampler tray temperatures were set to 50°C and 10°C, respectively. Mobile phases were made up of 20 mM ammonium acetate pH 5.5 in (A) H_2O/CH_3CN (95:5) and in (B) H_2O/CH_3CN (5:95). Gradient conditions were as follows: 0–2 min, B = 5%; 2–7 min, B = 5%–90%; 7–9 min, B = 90%; 9–10 min, B = 90%–5%; 10–15 min, B = 5%. The flow rate was maintained at 350 μL/min. A software-controlled divert valve was used to transfer eluent from 0–4.8 min and from 6.0–15 min of each chromatographic run to waste. The total chromatographic run time was 15 min. The sample injection volume was 10 μL. The autosampler injection valve and the sample injection needle were flushed and washed sequentially with mobile phase B (1 mL) and mobile phase A (2 mL) between each injection

Tandem mass spectrometric detection

The mass spectrometer was operated in positive ion mode. Quantitation was based on multiple reaction monitoring (MRM) detection of dansyl derivatives (tryptophan-d_0: *m/z* 438 → 170, 28 V; tryptophan-d_5: *m/z* 443 → 170, 24 V; kynurenine-d_0: *m/z* 442 → 170, 36 V; kynurenine-d_4: *m/z* 446 → 170, 32 V). The following optimized parameters were used for the detection of analytes and internal standards: N_2 sheath gas 45 psi; N_2 auxiliary gas 25 psi; spray voltage 5.0 kV; capillary temperature 280°C; capillary offset 35 V, tube lense offset 150 V, Ar collision gas 1.5 mtorr; scan time 50 ms; Q1/Q3 peak width at half-maximum 0.7 *m/z*.

Sample processing

Aliquots of thawed serum (50 μL) were transferred to clean microcentrifuge tubes and spiked with internal standards tryptophan-d_5 (5 μL) and kynurenine-d_4 (5 μL). Spiked serum was lightly vortexed, allowed to stand at room temperature for 15–20 min, and deproteinized with 75 μL of 2-propanol. Samples were then cooled to −20°C for 45–60 min, and precipitated proteins were removed by centrifugation (18,000 x *g*, 30 min, 5°C). The clear supernatant of each sample was transferred to a membrane dialysis cartridge (5000 MWCO) and filtered at 10°C for 6-8 h (10,000 x *g*). The filtrate was evaporated under a gentle stream of N_2 gas. The residue was reconstituted in 80 μL of H_2O/CH_3CN (1:1) containing 20 mM dansyl chloride and 100 mM $NaHCO_3$ (pH 8.0), and lightly vortexed for 20 min at room temperature. Following derivatization, the samples were diluted with 120 μL H_2O and centrifuged to remove particulates (18,000 x g, 22°C, 20 min). The clear supernatant was transferred to 200 μL silanized autosampler vials equipped with Teflon-lined bonded rubber septa.

LC/UV based quantification of kynurenine

The LC/UV method was used for the quantification of serum kynurenine following exogenous L-kynurenine administration as reported by Veres G et al. (Veres et al., 2015). Briefly, 3-nitro-L-tyrosine (3-NLT) was used as an internal standard and added to a final concentration of 3 μM to 80 μl of serum. Serum samples were acidified with an equal volume of 5% perchloric acid and centrifuged at 12,000 xg for 10 min at 4°C. The supernatant was removed and kynurenine was separated by high performance liquid chromatography (HPLC) coupled with UV detection on a 4.6 × 150 mm, 3 μm C-18 column (Acclaim 120) kept at 30°C. Elution was performed with 15 mM ammonium formate, 10% acetonitrile, pH 4.0, at flow rate of 0.7 ml/min. Both kynurenine and 3-NLT were detected by measuring the absorbance at 360 nm. Serum kynurenine was quantified using standard curves built from dilutions of a kynurenine standard that were treated like the serum samples.

HPLC-MS/MS based measurement of kynurenine pathway metabolites

For extraction of metabolites from serum, each sample was mixed with extraction solvent (methanol-water, 80:20; v/v; cooled to −80°C) at 1:10 ratio and vortexed for 1 min. Samples were further incubated at −80°C overnight and then spun at 20,000 *xg* for 30 min. The supernatant was collected in a new tube and dried down using a SpeedVac concentrator (Thermo Savant). For extraction of metabolites from tissue, samples were homogenized in extraction solvent at 20 μL/1mg of tissue. A fifth of the homogenate was further diluted five times with extraction solvent in a new tube and vortexed for 1 min. Samples were incubated at −80°C overnight and then spun at 20,000 x*g* for 30 min. The supernatant was collected in a new tube and dried down using a SpeedVac concentrator (Thermo Savant). After reconstitution in 60% acetonitrile, samples were analyzed by High-Performance Liquid Chromatography and Triple-quadruple Mass Spectrometry and Tandem Mass Spectrometry (HPLC-MS/MS). Specifically, the system consisted of a Thermo TSQ in line with an electrospray source and a Vanquish (Thermo) UHPLC consisting of a binary pump, degasser, and auto-sampler outfitted with a XBridge C18 column (Waters, dimensions of 2.1 mm × 50 mm and a 3.5 μm particle size). The mobile phase A contained 95% (vol/vol) water, 5% (vol/vol) acetonitrile, 20 mM ammonium hydroxide, 20 mM ammonium acetate, pH = 9.0; B was 100% Acetonitrile. The gradient was as following: 0 min, 15% A; 3 min, 45% A; 10 min, 60% A; 10.1-11 min, 75% A; 11.1 min, 15% A; 11.1-15 min, 15% A with a flow rate of 400 μL/min. In positive mode, the capillary of ESI source was set to 325°C, with sheath gas at 35 arbitrary units, auxiliary gas at 5 arbitrary units and the spray voltage at 3.5 kV. A selective reaction monitoring (SRM) of the protonated precursor ion and the related product ions were monitored. The transitions are listed as following: 3-hydroxy-anthranilic acid 154→136, 3-hydroxykynurenine 225→208, kynurenic acid 190→144, kynurenine 209→192, NAD^+ 664.078→428, picolinic acid 124→83, quinolinic acid 168.03→127, tryptophan 205→188, xanthurenic acid 206→160. Peak area was integrated, and data acquisition and analysis were carried out by Xcalibur 4.1 software and TraceFinder 4.1 software, respectively (both from Thermo Fisher Scientific).

Extraction and measurement of NAD^+

Intracellular NAD^+ and NADH levels in the kidney were determined by using the NAD/NADH Quantitation Colorimetric Kit (BioVision incorporation, San Francisco, CA, Catalog #K337) following the manufacturer's instruments. Briefly, 20-30 mg mouse kidneys were extracted in 500 μL NAD/NADH extraction buffer on ice. Protein concentration was measured with a BioRad protein assay (BioRad). The homogenate was filtered through 10 kDa molecular weight cut-off filters (Amicon Ultra, EMD Millipore) to remove NADH or NADPH consuming enzymes and subsequently assayed following manufacturer protocol. Finally, the results were obtained using a 96 well plate reader (BioTek) at the optical density of 450 nm.

Measurement of serum Epo

Serum Epo concentration was determined with a commercially available ELISA kit following the manufacturer provided instructions.

QUANTIFICATION AND STATISTICAL ANALYSIS

Statistical analyses were performed using the program "R" (https://cran.rproject.org/) or Prism 8 (GraphPad Software, La Jolla, CA). Two-tailed t test was used to calculate between-group differences while multiple comparisons were calculated by using one-way ANOVA with Sidak correction. For metabolites, statistical comparisons were performed by Welch's two sample t tests and random effects ANOVA. For RNA-seq, differential expression analysis was done by the R package edgeR. Statistical tests are referenced in the figure legends. A two-sided significance level of 5% was considered statistically significant. Results were reported as mean values ± SEM. n indicates biological replicates per experimental group.

Cell Reports, Volume *36*

Supplemental information

Hypoxic preconditioning protects against ischemic kidney injury through the IDO1/kynurenine pathway

Rafael Torosyan, Shengping Huang, Prashant V. Bommi, Ratnakar Tiwari, Si Young An, Michael Schonfeld, Ganeshkumar Rajendran, Matthew A. Kavanaugh, Benjamin Gibbs, Agnieszka D. Truax, Samuel Bohney, M. Wade Calcutt, Evan W. Kerr, Roberta Leonardi, Peng Gao, Navdeep S. Chandel, and Pinelopi P. Kapitsinou

Suppl. Figure 1

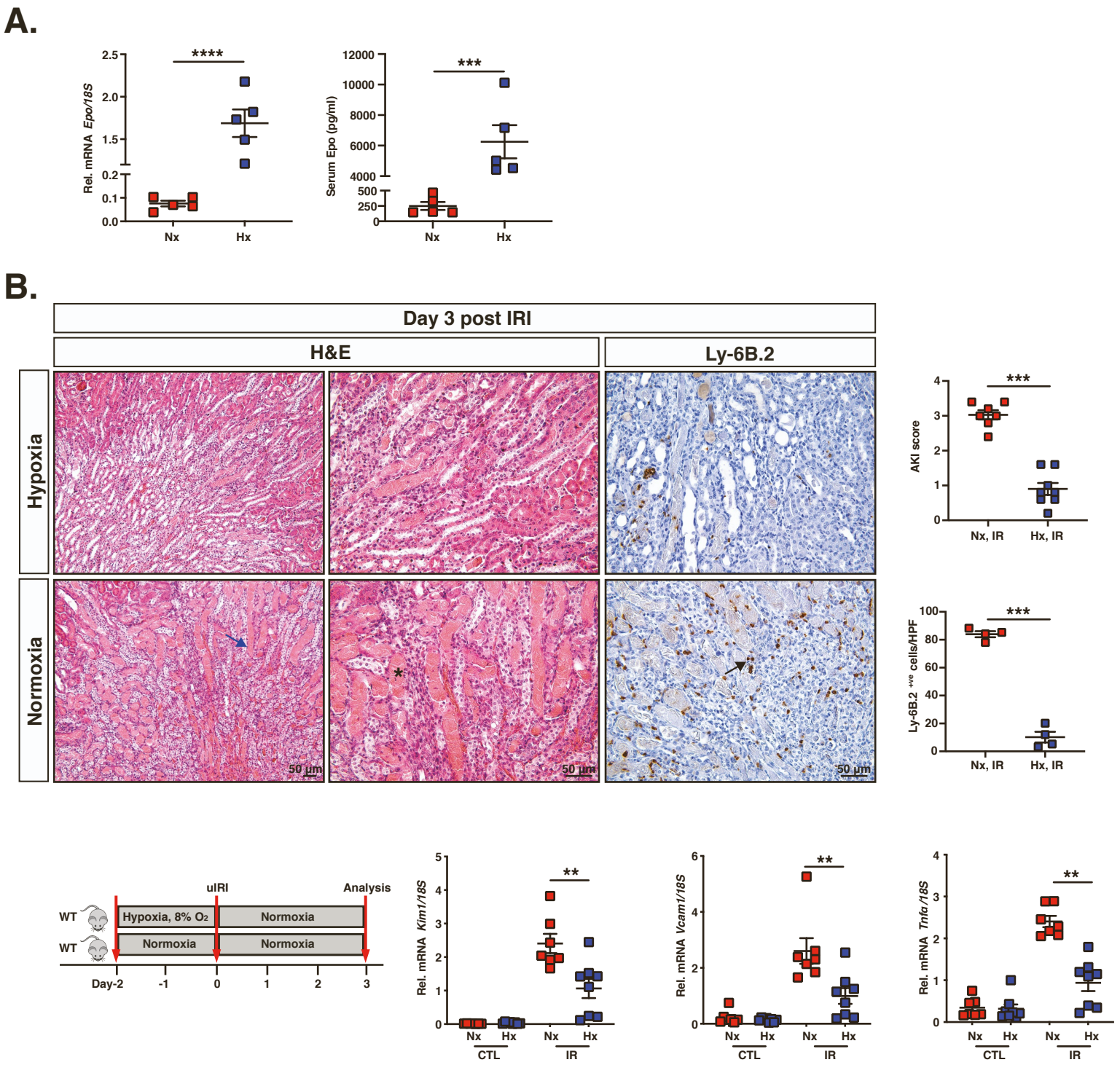

Figure S1, Related to Figure 1. Hypoxic preconditioning attenuates postischemic kidney injury and inflammation. (A) Shown are renal *Epo* mRNA levels (left graph) and serum Epo concentrations (right graph) in mice exposed to hypoxia **(**8% O_2, 2 days). (n=5). **(B)** Overview of the experimental protocol and representative images of H&E and Ly-6B.2-stained sections of injured kidneys from wild-type mice subjected to HP compared to normoxia 3 days after unilateral renal IRI. Arrow points to a dilated tubule; asterisk indicates a tubule with cast formation. Right panels demonstrate scoring of tubular injury (n=8-7) and quantification of Ly-6B.2^{+ve} cells/HPF in post-ischemic kidneys of the indicated experimental conditions (n=4). Bottom graphs show *Kim1, Vcam1, and Tnfa* mRNA levels in day 3 post-IRI and CTL kidneys from wild type mice subjected to HP compared to normoxia. (n=8-7). Error bars represent S.E.M; **, P<0.01; ***, P<0.001; ****, P<0.0001. Statistics were determined by two-tailed t-test for (**A**) and by one-way ANOVA with Sidak correction for (**B**). Scale bar indicates 50 μm. Hx, hypoxia; Nx, normoxia; uIRI, unilateral ischemia reperfusion injury; WT, wild-type; IR, kidney subjected to uIRI; CTL, contralateral kidney.

Suppl. Figure 2

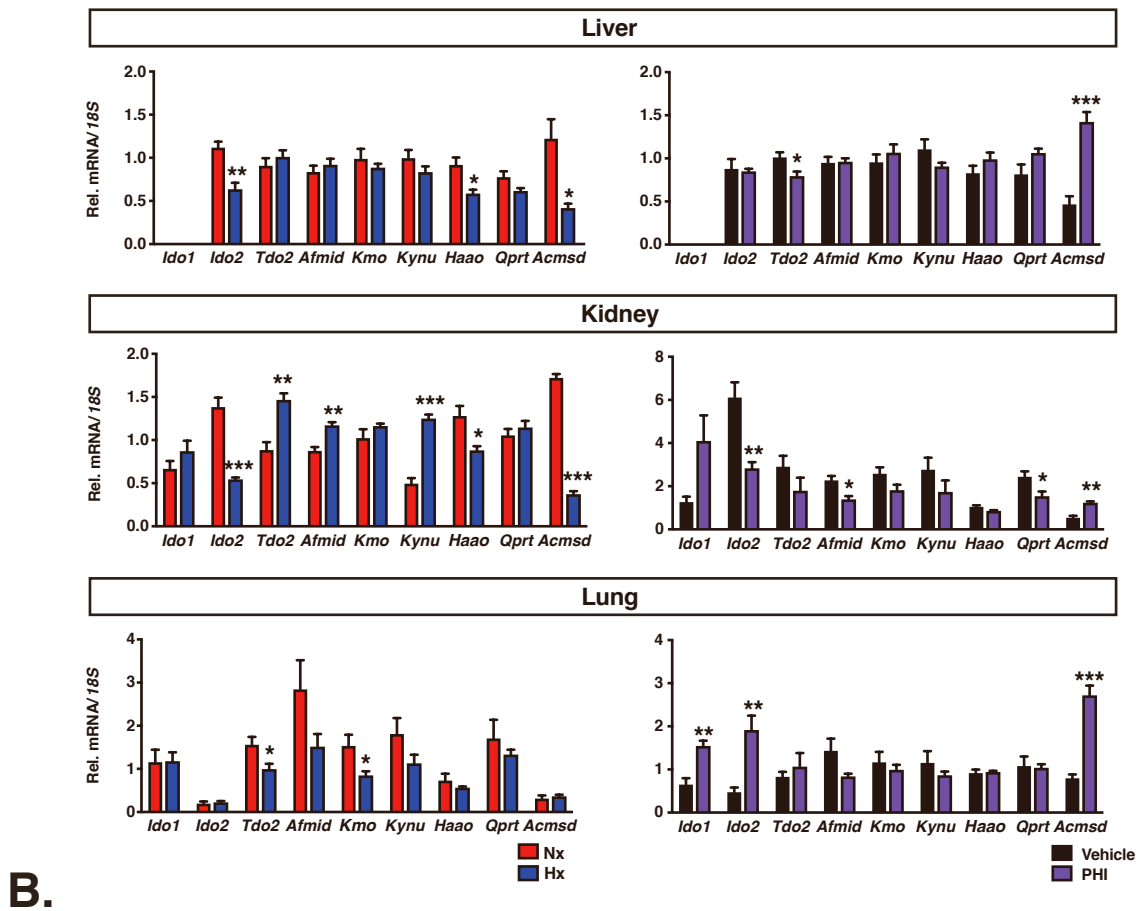

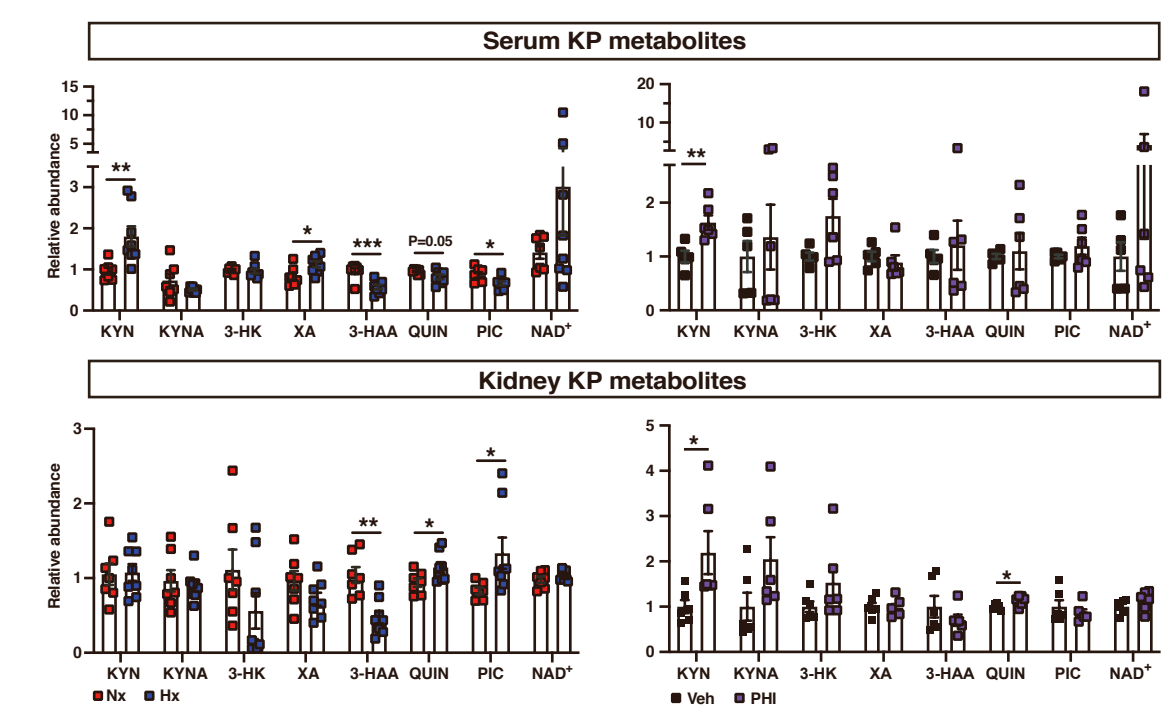

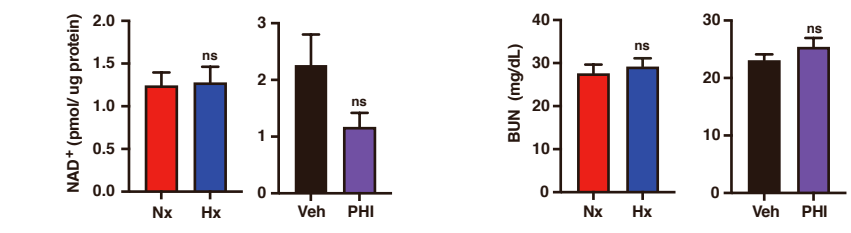

Figure S2, Related to Figure 2. Hypoxic preconditioning and pharmacologic PHD inhibition generate distinct transcriptional responses in kynurenine pathway genes in the liver, kidney and lung without altering kidney NAD^+ content. (A) Transcript levels of genes encoding KP enzymes following hypoxia exposure compared to normoxia and PHD inhibition compared to vehicle. RT-PCR analysis was performed in RNA extracted from livers (upper panels), kidneys (middle panels), and lungs (lower panels) (n=5). **(B)** Levels of serum and kidney KP metabolites in conditions indicated in (A) (n=7-8 for Hx vs Nx, n=6 for PHI vs vehicle). **(C)** Kidney NAD^+ levels (n=7 for Hx vs Nx, n=4 for PHI vs vehicle) and **(D)** serum BUN levels (n=8-7 for Hx vs Nx, n=10-7 for PHI vs vehicle). Error bars represent S.E.M; *, P<0.05; **, P<0.01; ***, P<0.001; ns, not statistically significant. Statistics were determined by two-tailed t-test. PHI, prolyl hydroxylase inhibitor. *Afmid,* arylformamidase; *Kmo,* kynurenine 3-monooxygenase*; Kynu,* kynurerinase; *Haao,* 3-hydroxyanthranilate 3,4-dioxygenase; *Qprt,* quinolinate phosphoribosyltransferase*; Acmsd,* alpha-amino-beta-carboxy-muconate-semialdehyde decarboxylase. KYN, kynurenine; KYNA, kynurenic acid; 3-HK, 3-hydroxykynurenine; XA, xanthurenic acid; 3-HAA, 3-hydroxyanthranilic acid; QUIN; quinolinic acid, PIC; picolinic acid. BUN, blood urea nitrogen.

Suppl. Figure 3

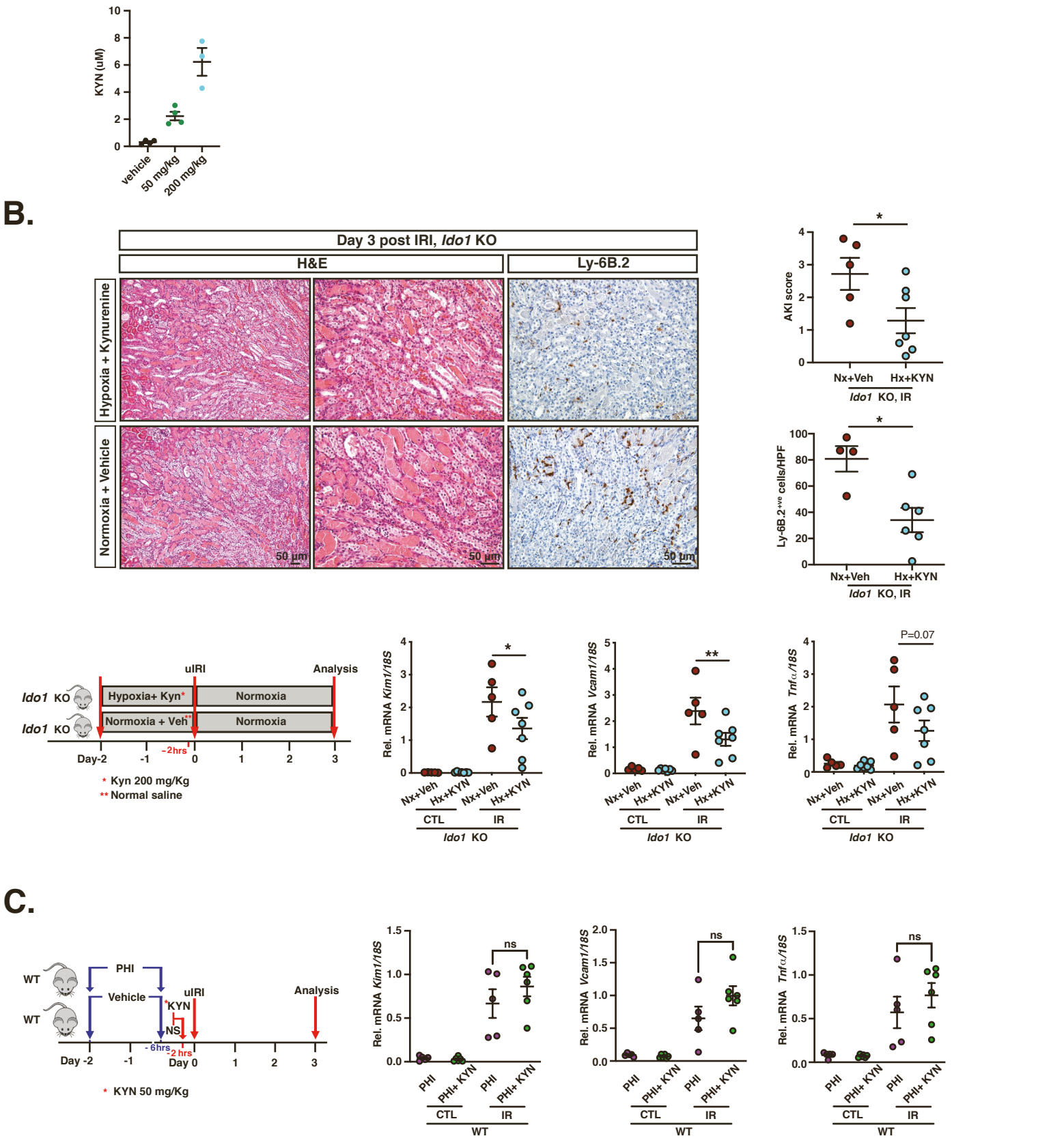

Figure S3, Related to Figure 3. Exogenous kynurenine administration restores the hypoxic preconditioning in mice lacking *Ido1*. **(A)** Serum kynurenine levels achieved at 2 hrs post i.p. administration of kynurenine at doses 50 mg/kg and 200 mg/kg compared to vehicle (normal saline). **(B)** Schematic of the experimental protocol, representative images of H&E and Ly-6B.2-stained sections of day 3 post-IRI kidneys from *Ido1* KO mice subjected to HP and i.p. kynurenine administration (200 mg/kg) compared to normoxic *Ido1* KO mice treated with vehicle. Right panels demonstrate scoring of tubular injury (n=6-8) and quantification of Ly-6B.2^{+ve} cells/HPF (n=4-6) in post-ischemic kidneys of the indicated experimental conditions. Bottom graphs show *Kim1, Vcam1*, *and Tnfa* mRNA levels in IR and CTL kidneys (n=5-7). **(C)** Schematic of the experimental protocol, in which animals were pretreated with a PHD inhibitor (at 2 days and 6 hrs prior to renal IRI) and received either one single injection of kynurenine (50 mg/kg) or normal saline 2 hrs prior to IRI. Right graphs show *Kim1, Vcam1*, *and Tnfa* transcript levels in IR and CTL kidneys (n=5-6) at the indicated experimental conditions. Error bars represent S.E.M. For AKI scores and Ly-6B.2^{+ve} cell counts, statistics were determined by two-tailed t-test. All other comparisons were performed by one-way ANOVA with Sidak correction. *, $P<0.05$; **, $P<0.01$; ns, not statistically significant. KYN, kynurenine. Scale bar indicates 50 μm.

Suppl. Figure 4

A.

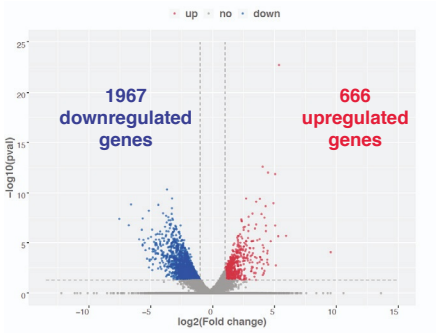

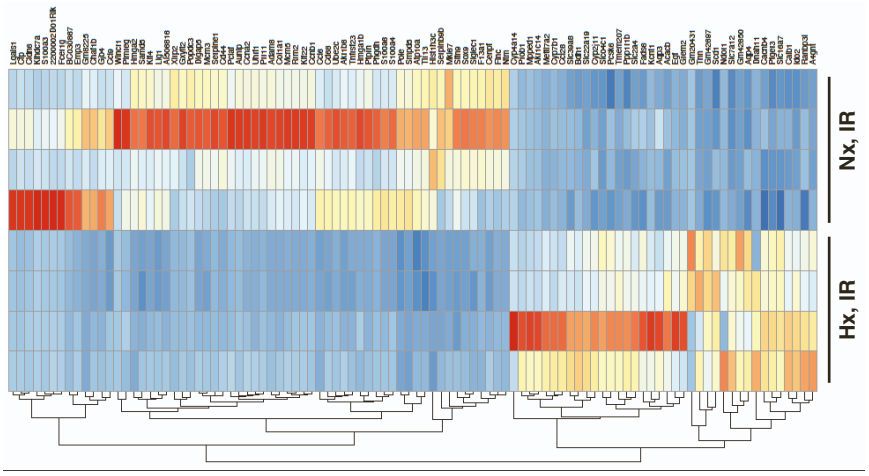

B.

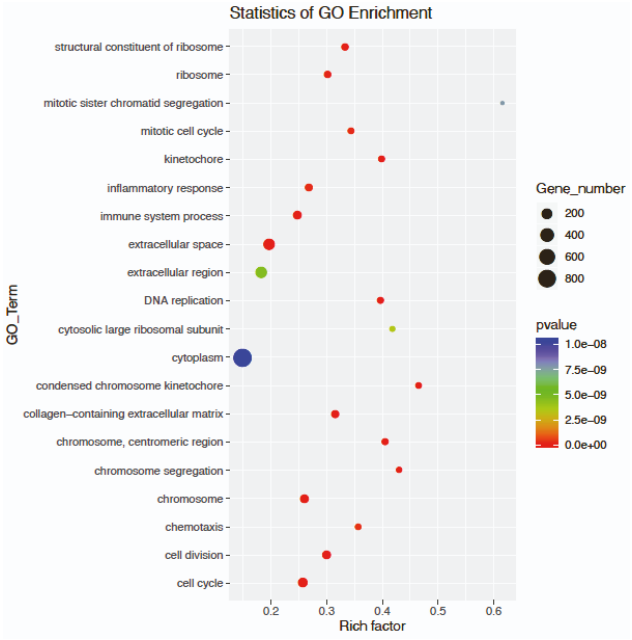

C.

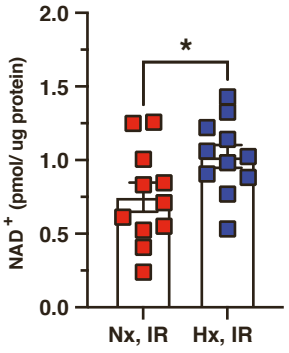

D.

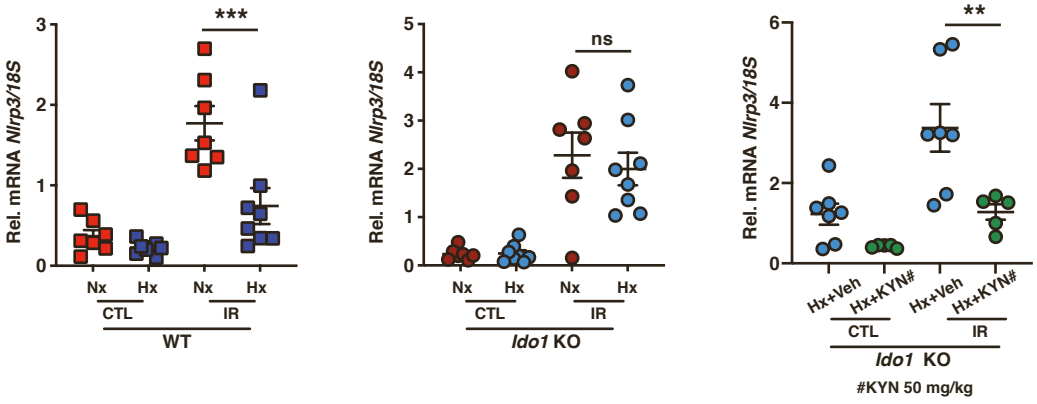

Figure S4, Related to Figure 4. RNA-sequencing performed in day 3 post-ischemic kidneys from wild type subjected to hypoxic preconditioning compared to normoxia. (A) (Left) Volcano plot of the differentially expressed genes (DEGs) in postischemic kidneys between the HP and the normoxia groups. Red indicates up-regulated genes, and blue indicates down-regulated genes. The grey area shows the gene expression below the threshold criteria (log2FC > 1 or <-1 and P value<0.05). (Right) Heat map of log10(FPKM) across all the samples using the top 100 most DEGs in post-ischemic kidneys subjected to HP compared to the normoxia group. Each column corresponds to a specific gene and each row corresponds to a sample. **(B)** The GO enrichment graph displays the top 20 pathways. The number of DEGs enriched in GO terms, p value, and rich factor are shown in scatterplot. Rich factor = (number of DEGs in GO term)/(total number of genes in GO term). **(C)** NAD^+ levels in postischemic kidney tissue from mice subjected to HP compared to normoxia (n=11/group, measured by colorimetric assay). **(D)** Shown are *Nlrp3* mRNA levels in day 3 post-ischemic and contralateral kidneys. Left graph: wild-type mice subjected to HP compared to normoxia (n=7-8); middle graph: *Ido1* KO mice subjected to HP compared to normoxia (n=7-8); right graph: *Ido1* KO mice subjected to HP and kynurenine administration compared to HP/vehicle treated *Ido1* KO mice (n=7-5). Error bars represent S.E.M; **, P<0.01; ***, P<0.001; ns, not statistically significant. Veh, vehicle; WT, wild-type; KYN, kynurenine.